

DTIC FILE COPY

②

GL-TR-90-0154

AD-A227 424

**Effects of a Descending Lithospheric Slab on Yield
Estimates of Aleutian Nuclear Tests**

**Three Dimensional Structure of Subducted Lithospheric Slabs
Constraints from the Amplitudes and Waveforms of S Waves**

Vernon F. Cormier

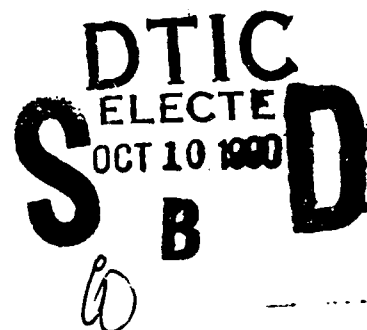
University of Connecticut
Department of Geology and Geophysics
Storrs, Connecticut 06269-2045

August 10, 1990

Scientific Report No. 2

Approved for public release; distribution unlimited

**GEOPHYSICS LABORATORY
AIR FORCE SYSTEMS COMMAND
UNITED STATES AIR FORCE
HANSCom AIR FORCE BASE, MASSACHUSETTS 01731-5000**

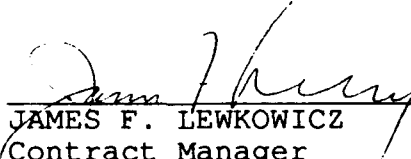



SPONSORED BY
Defense Advanced Research Projects Agency
Nuclear Monitoring Research Office
ARPA ORDER NO 5299

MONITORED BY
Geophysics Laboratory
F19628-88-K-0010

The views and conclusions contained in this document are those of the authors and should not be interpreted as representing the official policies, either expressed or implied, of the Defense Advanced Research Projects Agency or the U.S. Government.

This technical report has been reviewed and is approved for publication.


JAMES F. LEWKOWICZ
Contract Manager
Solid Earth Geophysics Branch
Earth Sciences Division


JAMES F. LEWKOWICZ
Branch Chief
Solid Earth Geophysics Branch
Earth Sciences Division

FOR THE COMMANDER


DONALD H. ECKHARDT, Director
Earth Sciences Division

This report has been reviewed by the ESD Public Affairs Office (PA) and is releasable to the National Technical Information Service (NTIS).

Qualified requestors may obtain additional copies from the Defense Technical Information Center. All others should apply to the National Technical Information Service.

If your address has changed, or if you wish to be removed from the mailing list, or if the addressee is no longer employed by your organization, please notify GL/IMA, Hanscom AFB, MA 01731-5000. This will assist us in maintaining a current mailing list.

Do not return copies of this report unless contractual obligations or notices on a specific document requires that it be returned.

REPORT DOCUMENTATION PAGE

Form Approved
OMB No. 0704-0188

Public reporting burden for this collection of information is estimated to average 1 hour per response, including the time for reviewing instructions, searching existing data sources, gathering and maintaining the data needed, and completing and reviewing the collection of information. Send comments regarding this burden estimate or any other aspect of this collection of information, including suggestions for reducing this burden, to Washington Headquarters Services, Directorate for Information Operations and Reports, 1215 Jefferson Davis Highway, Suite 1204, Arlington, VA 22202-4302, and to the Office of Management and Budget, Paperwork Reduction Project (0704-0188), Washington, DC 20503.

1. AGENCY USE ONLY (Leave blank)

2. REPORT DATE

August 10, 1990

3. REPORT TYPE AND DATES COVERED

Scientific #2

4. TITLE AND SUBTITLE Effects of a Descending Lithospheric Slab on Yield Estimates of Aleutian Nuclear Tests. Three Dimensional Structure of Subducted Lithospheric Slabs Constraints from the Amplitudes and Waveforms of S Waves.

5. FUNDING NUMBERS

PE 61101E

PR 8A10 TA DA WU AE

6. AUTHOR(S)

Vernon F. Cormier

Contract F19628-88-K-0010

7. PERFORMING ORGANIZATION NAME(S) AND ADDRESS(ES)

University of Connecticut
Department of Geology and Geophysics
Storrs, CT 06269-2045

8. PERFORMING ORGANIZATION
REPORT NUMBER

9. SPONSORING / MONITORING AGENCY NAME(S) AND ADDRESS(ES)

Geophysics Laboratory
Hanscom AFB, MA 01731-5000

10. SPONSORING / MONITORING
AGENCY REPORT NUMBER

GL-TR-90-0154

Contract Manager: James Lewkowicz/LWH

11. SUPPLEMENTARY NOTES

12a. DISTRIBUTION / AVAILABILITY STATEMENT

Approved for public release; distribution unlimited

12b. DISTRIBUTION CODE

13. ABSTRACT (Maximum 200 words)

Theoretical amplitudes and travel times were computed using vicinity ray tracing in several different types of descending slab models, including two new models proposed for the Aleutian slab by Boyd and Creager (1989). In agreement with a similar study of focusing and defocusing at the Nevada Test Site (Cormier, 1987), it was found that amplitudes do not correlate with travel times on a point for point basis, although broad regional anomalies in amplitudes correlate with broad regional anomalies in travel times. For a shallow focus source placed located to correspond to the relative locations of the Amchitka tests, a regional variation in P amplitudes was found that is similar to those found in the Study by Sleep (1973). Negative m_b residual of -0.2 to -0.3 units are predicted for in a broad azimuthal range on the dipping side of the slab. Lowest amplitudes are predicted at due North azimuths in the range of 70 to 90 great circle degrees. Smaller zones of positive m_b residual are predicted in the distance range 42 to 53 great circle range at due North azimuth, which is also a zone of P wave multipathing. Multipathing is also predicted PcP over small geographic regions perpendicular to the strike of the slab near 12 great circle degrees.

Many experiments were conducted in varying source location within and near slab structure. These demonstrate that multipathing is most easily induced if the source is located close to the high gradient zone defining the top of the slab.

Continued on back side.

14. SUBJECT TERMS

Effects of a Descending Lithospheric Slab on Yield Estimates of Aleutian Tests

15. NUMBER OF PAGES

70

16. PRICE CODE

17. SECURITY CLASSIFICATION
OF REPORT

UNCLASSIFIED

18. SECURITY CLASSIFICATION
OF THIS PAGE

UNCLASSIFIED

19. SECURITY CLASSIFICATION
OF ABSTRACT

UNCLASSIFIED

20. LIMITATION OF ABSTRACT

SAR

Abstract Continued

S and ScS amplitudes and travel times were also computed in these models, as part of a related study funded by NSF. For earthquakes located within slabs, it was assumed that regions of defocussing correspond to regions of maximum broadening and complexity in S waves. Slabs that thicken or have a reduced velocity contrast below, 650 km depth predict a different regional pattern of S and ScS waveform broadening compared to that predicted by slabs that penetrate the 650 km discontinuity for a long distance as a thin tabular structure. Data from the Kuril-Kamchatka slab are consistent with advective thickening or reduced velocity contrast below 650 km depth. The particular pattern of S and ScS waveform broadening in North America is more likely to be a consequence of a slab effect than an attenuation effect.

TABLE OF CONTENTS

I. Technical Summary	v
II. Theoretical Amplitude Anomalies of Aleutian Nuclear Tests	1
III. Three-dimensional structure of Subducted Lithospheric Slabs: Constraints from the Amplitudes and Waveforms of S Waves by Vernon F. Cormier and Woohan Kim	
Abstract	10
Introduction	12
Calculation of Slab Effects on Waveforms	13
Focusing and Defocusing of Experiments	21
Bent Slabs and Multipathing	32
Conclusions	34
References	37
Figures (1-14)	39



Accession For	
NTIS GRA&I	<input checked="" type="checkbox"/>
DTIC TAB	<input type="checkbox"/>
Unannounced	<input type="checkbox"/>
Justification	
By _____	
Distribution/	
Availability Codes	
Dist	Avail and/or Special
A-1	

TECHNICAL SUMMARY

The objective of this project is to determine the yield bias of underground nuclear tests induced by the presence of a high velocity descending slab beneath the test site. Specifically, the effect of the Aleutian slab is being investigated on the US underground tests Longshot, Milrow, and Cannikan. P wave seismograms will be synthesized using dynamic ray tracing and superposition of Gaussian beams in three-dimensional models of the Aleutian slab determined from P travel time delays. Focusing and defocusing and multipathing at teleseismic distances will be evaluated by comparison of observed with synthetic seismograms of the Aleutian tests.

Theoretical amplitudes and travel times were computed using vicinity ray tracing in several different types of descending slab models, including two new models proposed for the Aleutian slab by Boyd and Creager (1989). In agreement with a similar study of focusing and defocusing at the Nevada Test Site (Cormier, 1987), it was found that amplitudes do not correlate with travel times on a point for point basis, although broad regional anomalies in amplitudes correlate with broad regional anomalies in travel times. For a shallow focus source placed located to correspond to the relative locations of the Amchitka tests, a regional variation in P amplitudes was found that is similar to those found in the Study by Sleep (1973). Negative m_b residuals of -.2 to -.3 units are predicted for in a broad azimuthal range on the dipping side of the slab. Lowest amplitudes are predicted at due North azimuths in the range of 70 to 90 great circle degrees. Smaller zones of positive m_b residual are predicted in the distance range 42 to 53 great circle range at due North azimuth, which is also a zone of P wave multipathing. Multipathing is also predicted PcP over small geographic regions perpendicular to the strike of the slab near 12 great circle degrees.

Many experiments were conducted in varying source location within and near slab structure. These demonstrate that multipathing is most easily induced if the source is located close to the high gradient zone defining the top of the slab.

S and ScS amplitudes and travel times were also computed in these models, as part of a related study funded by NSF. For earthquakes located within slabs, it was assumed that regions of defocussing correspond to regions of

maximum broadening and complexity in S waves. Slabs that thicken or have a reduced velocity contrast below 650 km depth predict a different regional pattern of S and ScS waveform broadening compared to that predicted by slabs that penetrate the 650 km discontinuity for a long distance as a thin tabular structure. Data from the Kuril-Kamchatka slab are consistent with advective thickening or reduced velocity contrast below 650 km depth. The particular pattern of S and ScS waveform broadening in North America is more likely to be a consequence of a slab effect than an attenuation effect.

THEORETICAL AMPLITUDE ANOMALIES OF ALEUTIAN NUCLEAR TESTS

Theoretical amplitudes and travel times were computed using vicinity ray tracing (Kim and Cormier, 1990) in the long slab model of Body and Creager (1989) for the Aleutian slab for source positions corresponding to underground nuclear tests in the island ridge adjacent to the slab. In constructing the model shown in Figure 1, the raw thermal model was obtained from Creager (personal communication) and converted to a P velocity model by assuming the temperature derivative of P velocity used by Boyd and Creager, $dV_P/dT = 0.5 \text{ ms}^{-1} \text{ K}^{-1}$. Details of the amplitude calculation are described in the section following this one, which also describes experiments calculating slab focusing and defocusing and in several different types of slab models and source positions within the slab.

Figure 2 shows P and PcP rays predicted for Amchitka tests in the Boyd and Creager model. The rays are shown for a 2-D cross section, perpendicular to the strike of the slab. Multipathing can be observed at the great circle distances 42° to 53° for P waves and around 12° for PcP waves.

Amplitude and travel times were calculated in models with and without the slab using PREM as a reference model. P amplitude anomalies are shown in figure 3, contoured in m_b residuals. A geographic plotting convention is used rather than a focal sphere plot. The epicenter is at the center of the sphere, the inner circle corresponds to the area at distances less than or equal to 35° , the outer circle corresponds to core grazing distances.

The amplitude variations in Figure 3 roughly agree with the data shown in Figure 10 of Sleep's (1973) study. Highest amplitudes occur around an annular region at 42° to 53° . Low amplitudes occur at longer distances outside this ring, nearly everywhere on the dipping side of the slab. Peak m_b residuals are bounded by 0.3 m_b units. The lowest amplitudes occur at azimuths due North, perpendicular to the strike of the slab, at ranges exceeding 53° . This is the region in which evidence of pulse broadening has been reported in long period and broadband waveforms from shallow focus Aleutian events (Engdahl et al., 1989). Since this is a region of strong defocusing (-0.3 m_b residual), the pulse broadening may likely be caused by slab diffraction.

Large anomalies in PcP amplitudes of +0.6 log amplitude units occur in two symmetric geographic regions at 12° range (Figure 4). Multipathing of

PcP is predicted to occur in these regions. The largest amplitude multipath was chosen for contouring. Core reflected phases such as PcP and ScS are particularly sensitive to steeply dipping slab structures and can be used as effective tools in discriminating between possible deep slab structures.

Predicted travel time anomalies of the P waves from Aleutian tests are shown in Figure 5. Travel time anomalies are uniformly negative due to fact that all rays interact to some extent with the high velocity slab structure. The fast travel time correlate with low amplitudes in a broad regional sense, but many exceptions to the broad correlation can be seen in a comparison with the amplitude anomalies shown in Figure 3.

In summary, forward modeling in recently proposed models of the Aleutian slab is generally consistent with the predictions obtained in earlier studies by Davies and Julian (1972) and Sleep (1973). In continued work in this project, we will make an effort to include additional digital waveform data not available to these earlier studies in order to confirm both their results as well as to investigate the effect of the Aleutian slab on P waveform broadening and complexity.

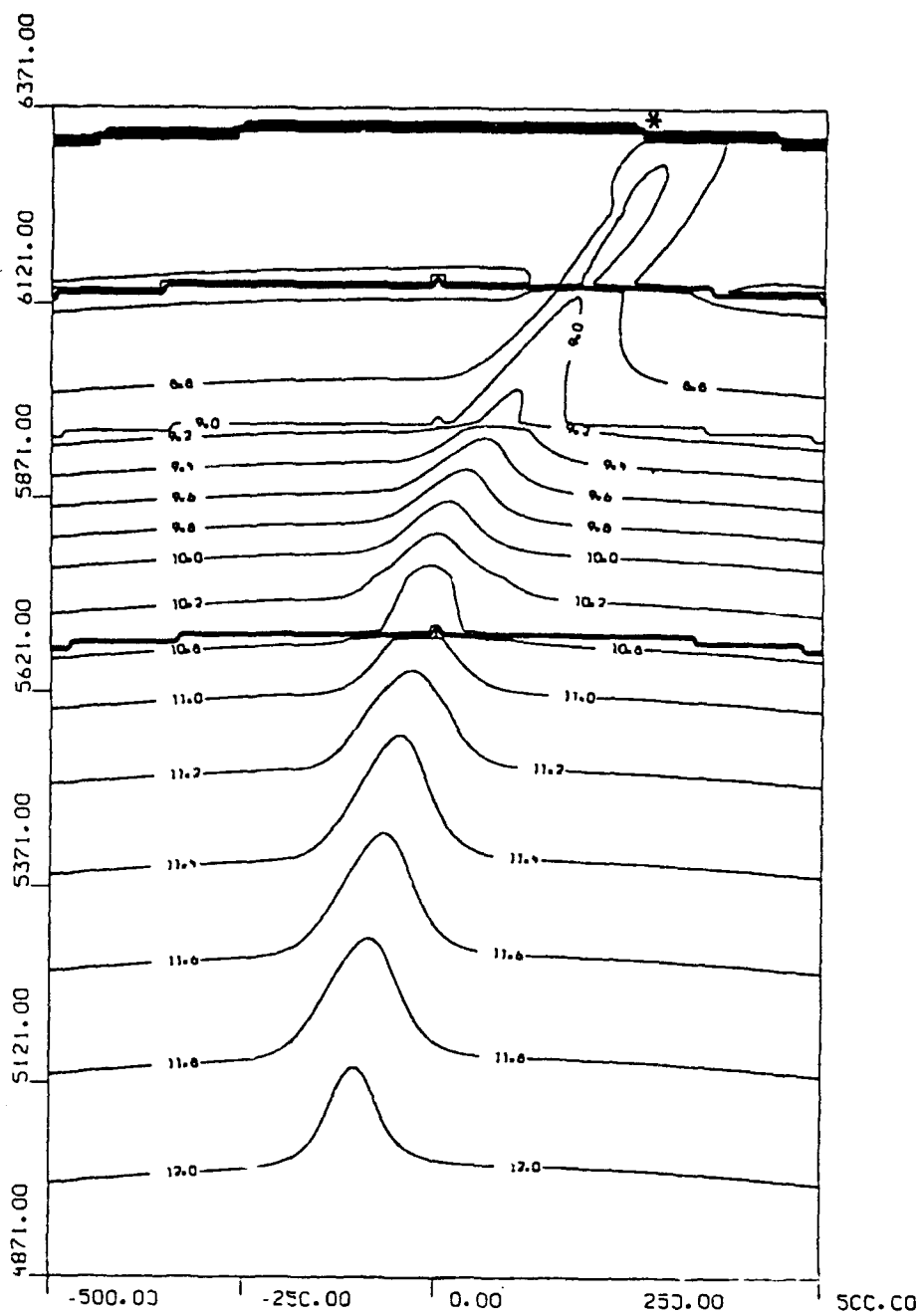


Figure 1: P velocity model of the Aleutian slab in the vicinity of the Amchitka test site determined by Boyd and Creager (1989)

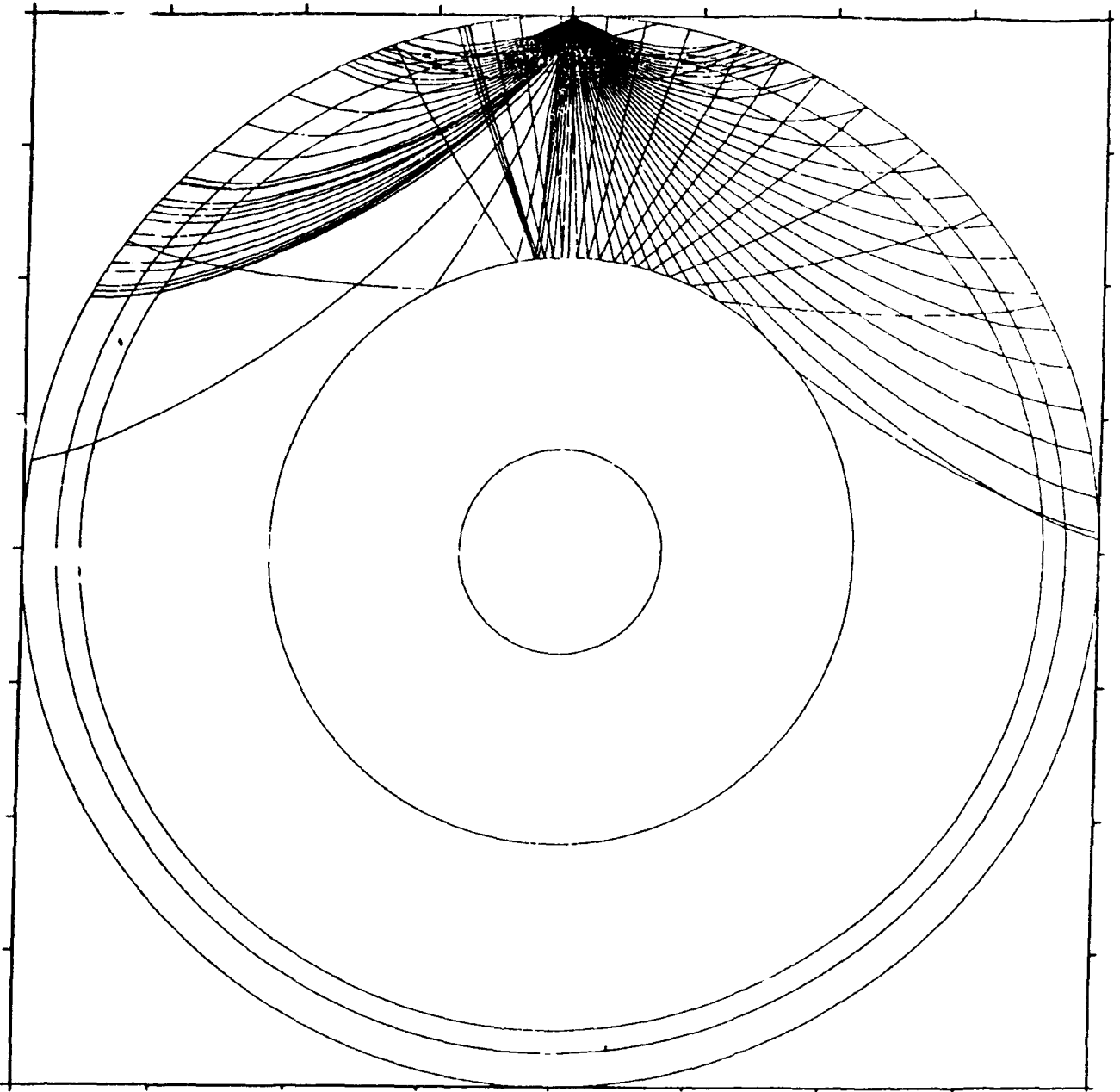


Figure 2: P and PcP ray trajectories in a plane perpendicular to the strike of the Aleutian slab model shown in Figure 1.

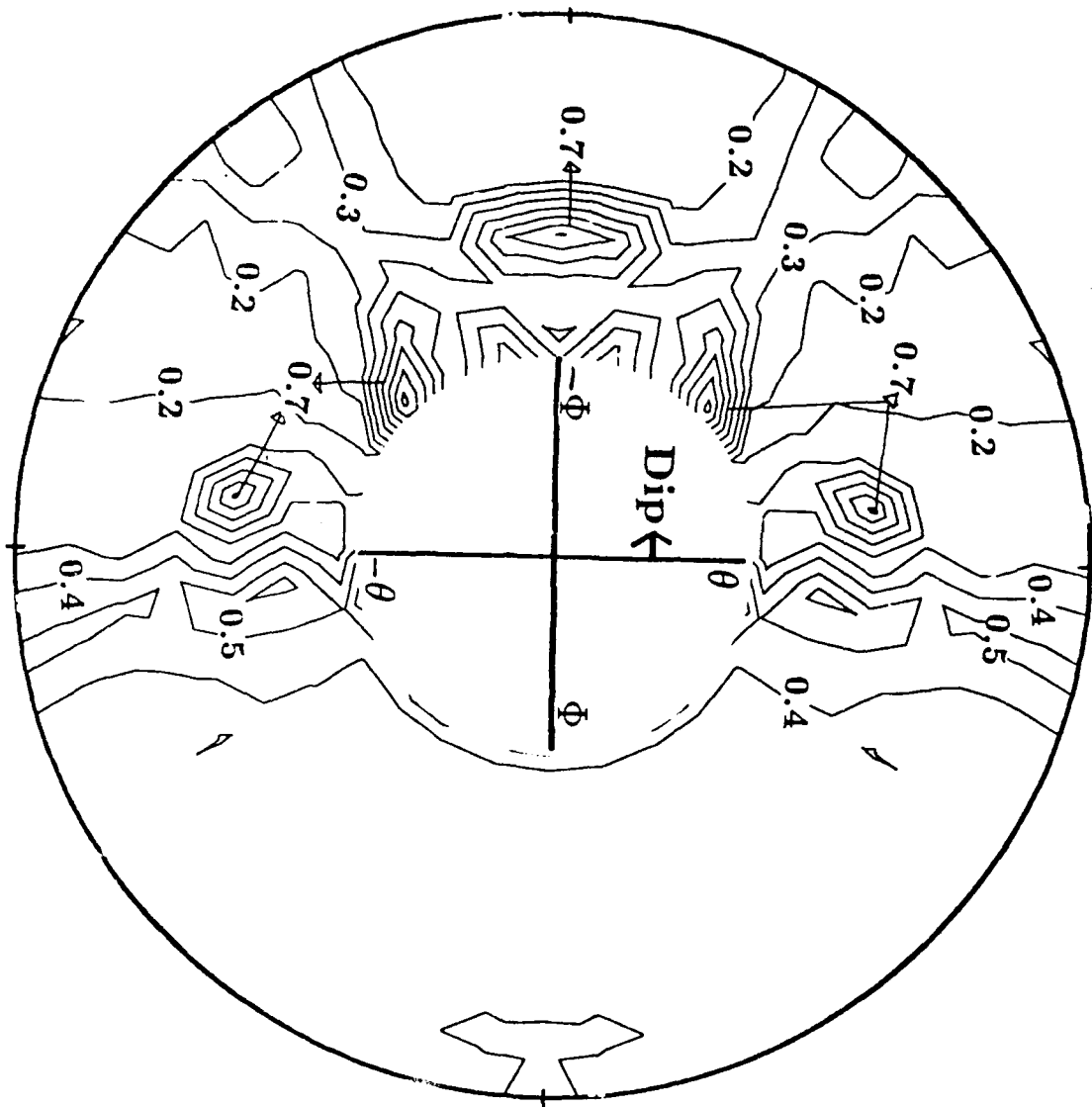


Figure 3: Predicted P amplitude anomalies for a source located as shown in the model shown in Figure 1. Anomalies are contoured in m_b units. An equal area geographic projection has been used, with the inner radius corresponding to 40° distance and the outer radius to 90° degrees distance.

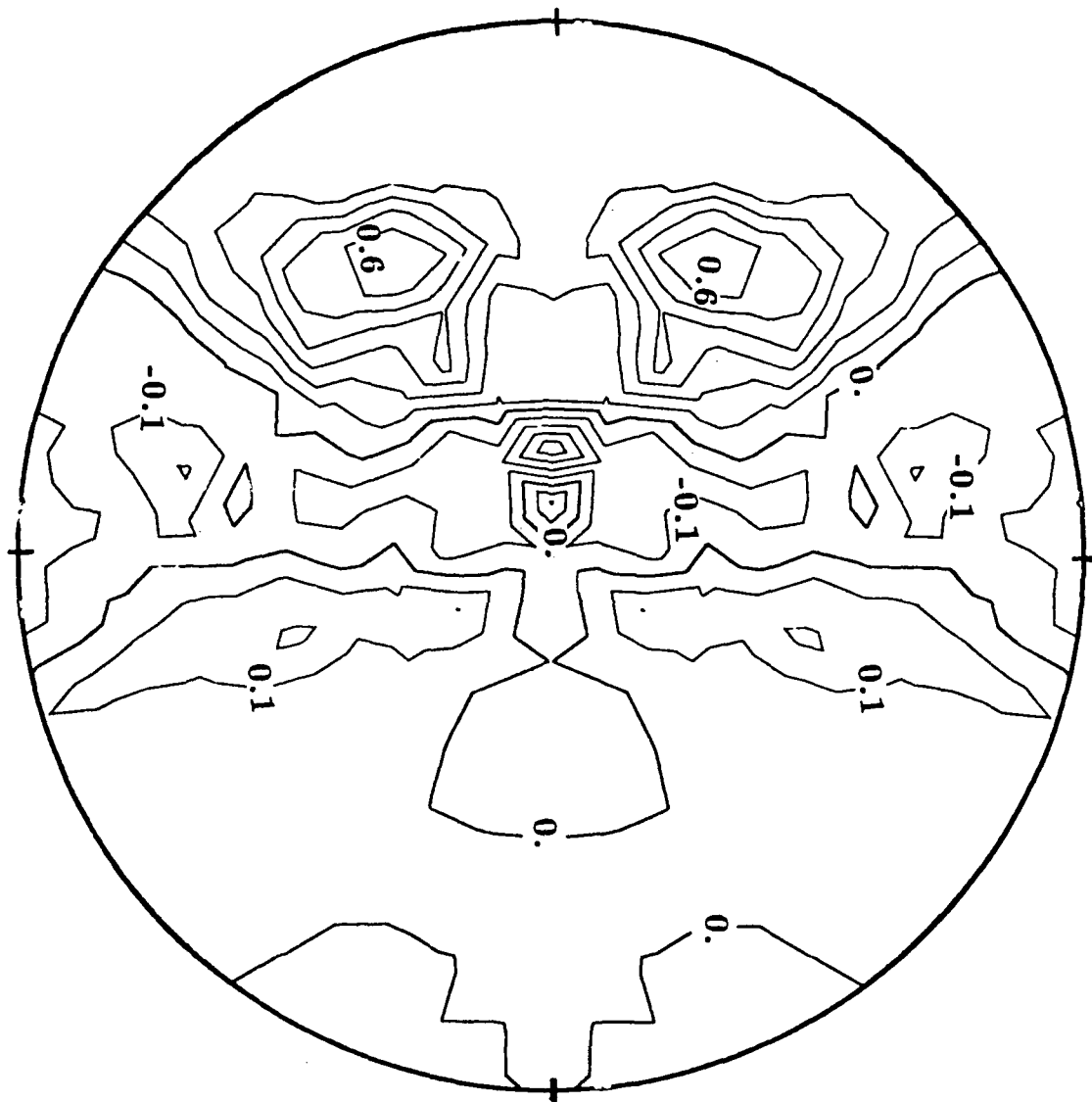


Figure 4: Predicted PcP amplitude anomalies for a source located as shown in the model shown in Figure 1. Plotting is an equal area geographic projection with the outer radius corresponding to 90° degrees distance.

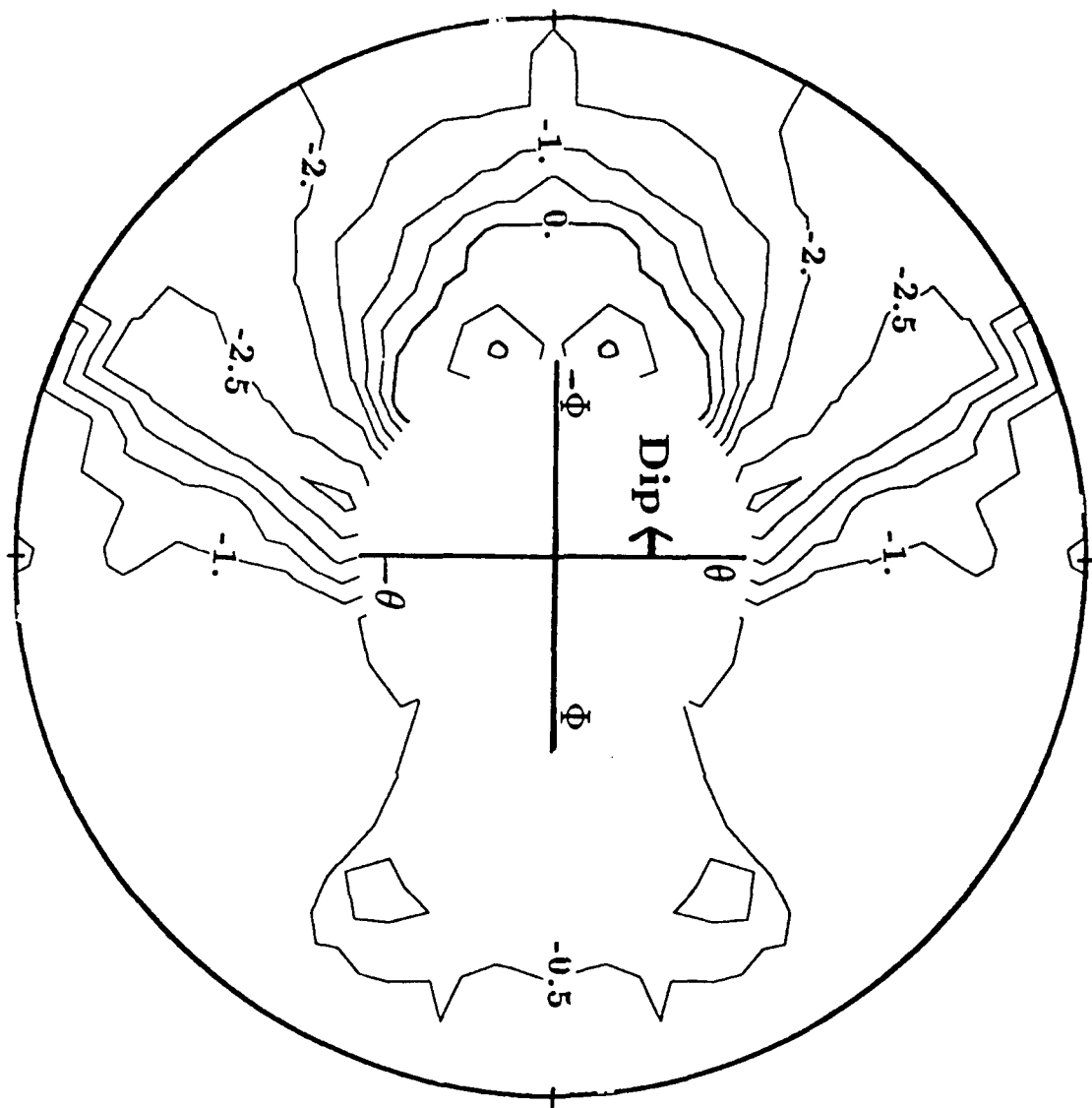


Figure 5: Predicted P travel time anomalies in seconds for a source located as shown in the model in Figure 1. Anomalies are calculated relative to PREM.

Three-dimensional Modeling of Subducted Lithospheric
Slabs from the Amplitudes and Waveforms of S Waves

Vernon F. Cormier and Woohan Kim
Department of Geology and Geophysics
University of Connecticut
Storrs, CT 06269-2045

Submitted to *Journal of Geophysical Research*

Abstract

A modified form of dynamic ray tracing is used to predict travel times, geometric spreading, and waveform distortions of S waves radiated by deep focus earthquakes located in several different thermal models of slab structure proposed below 650 km depth. By assuming that the peak displacement amplitudes calculated from frequency independent ray theory are the same as those calculated from finite difference studies, the regional dependence of waveform broadening due to the frequency dependent phenomenon of slab diffraction may be predicted. Using this hypothesis the following are predicted:

(1) Steeply dipping slabs that penetrate the 650 km discontinuity, with little advective thickening and a strong temperature contrast from the surrounding mantle, produce fast travel times, low amplitudes, and slab diffraction of primarily ScS waveforms in nearly a 180 degree azimuthal sector on the dipping side of the slab. These effects are much smaller in S waves except along azimuths close to the strike of the slab.

(2) Slabs that advectively thicken and/or suffer a strong change in temperature contrast below 650 km depth predict fast travel times, low amplitudes, and waveform broadening in S but not ScS waves along azimuths principally along the strike of the slab. The S anomalies increase as the great circle range decreases below 60 degrees.

(3) S and ScS waveforms and travel times observed from deep focus earthquakes occurring within the Kuril-Kamchatka slab are more consistent with (2) than (1). This suggests that while a slab structure or thermal anomaly likely exists below 650 km depth, it experiences some advective thickening below this depth.

Introduction

The travel times of P and S waves from deep focus earthquakes have suggested that slabs may penetrate into the deep mantle of the Earth below 650 km depth. This depth is close to the deepest recorded earthquakes and also coincides with a rapid, probably discontinuous increase in seismic velocities and density.

It is important to determine whether the cutoff in seismicity and the changes in physical properties of the mantle at 650 km depth correspond to a solid-solid phase change and/or a compositional change in the mantle at this depth. If it is a compositional change or if the change in physical properties greatly reduces the negative buoyancy of the slab, then the likely mode of mantle convection would be two-layered rather than a single layer between the asthenosphere and core-mantle boundary. In this case, one would expect the slab not to penetrate very far beyond 650 km depth and to suffer some deformation, advective thickening, or rapid diminution and assimilation into the lower mantle below this depth. If this not the case, the slab may penetrate below 650 km depth with little change in in shape.

To answer these questions, we conducted a series of experiments on the effects of several proposed slab structures in the lower mantle on the waveforms and amplitudes of seismic body waves. It is shown that the waveforms and amplitudes of body waves can provide constraints on slab structure independent of travel times. The results of these tests demonstrate that combined waveform and travel time data from deep focus earthquakes may be able to determine the nature of slab deformation near 650 km depth and thereby constrain the types of changes in physical properties of the mantle at this depth.

Calculation of Slab Effects on Waveforms

Previous Studies

General. Slab structure can affect waveforms and amplitudes as well as the travel times of body waves radiated by deep focus earthquakes. The waveform effects include focusing and defocusing, multipathing, and diffraction (Sleep, 1973; Davies and Julian, 1972; Vidale, 1987; Cormier, 1989; Silver and Chan, 1986; Engdahl et al., 1989; Vidale and Garcia-Lopez, 1988; Weber, 1990).

Gaussian beams. In an earlier study (Cormier, 1989), the frequency dependent effects of slab diffraction were approximately modeled using a superposition of Gaussian

beams. In a three-dimensional model, the beam superposition required several hundred dynamically traced rays to synthesize each body wave. To better approximate the Fresnel zone responsible for slab diffraction, beams were shot reciprocally from receiver to source rather than from the source to the receiver. An earth flattening transformation was assumed to simplify the conversion between the Cartesian coordinates, in which the model was specified, and the ray centered coordinates, in which the dynamic ray tracing equations were specified.

The limitation of the Gaussian beam method in the synthesis of the frequency dependent slab diffraction is associated more with its inability to properly describe the frequency dependence of the Fresnel zone in the source region than with any failure of the asymptotic and paraxial approximations in the spatially varying slab structure. Most of the proposed thermal models of slab structure are sufficiently smooth and slowly varying for both asymptotic and paraxial approximations to remain accurate in the frequency band of interest to broad band body waves. If beams are shot from the source to the receiver, their superposition simply reproduces the predictions of geometric ray theory, i.e., the frequency independent amplitudes determined from geometric spreading. This is because the class of ray paths included in the superposition excludes rays at grazing incidence to the high gradient zones defining the boundaries of the slab.

It is possible, however, to include these rays by shooting beams reciprocally from the receiver to the source. In this case, the superposition will produce broadened waveforms due to slab diffraction in a large geographic region on the dipping side of the slab. The waveform broadening vanishes as beam widths are decreased and/or the frequency band of synthesis increases.

The slab problem demonstrates that Gaussian beams satisfy reciprocity only in the limit of geometric ray theory in which beam widths become much narrower than those needed to describe properly the frequency dependence of the Fresnel zone responsible for slab diffraction. For these reasons, the Cormier (1989) study employed a reciprocal source-receiver geometry and calibrated beam parameters by comparing waveforms synthesized by beam superposition in three-dimensions with waveforms synthesized by the finite difference method in two-dimensions (Vidale, 1987; Witte, 1987). Because the beam method fails reciprocity and is limited in its ability to describe properly the Fresnel zone in the vicinity of the source region, it was deemed inappropriate at this time to apply superposition of Gaussian beams in a more comprehensive study of slab diffraction. Many valuable insights on slab structure, however, can be gained by a study of the focusing and defocusing effects of slabs predicted by simple geometric ray theory, and these

effects can be accurately calculated by dynamic ray tracing and conventional beam superposition.

This Study

Amplitudes and waveform complexity due to multipathing. In the present study, a modified form of dynamic ray tracing is applied in a spherical model to calculate peak amplitudes, travel times, and $\pi/2$ phase shifts induced by slab structure. Although this approach ignores frequency dependent effects and overestimates peak amplitudes in the vicinity of caustics, it allows a rapid reconnaissance of the principal effects of slab structures while including some advances over similar earlier studies. The estimates of geometric spreading should be more accurate in principal than those obtained in studies that calculate spreading from the differential area of closely spaced rays. The $\pi/2$ phase shifts introduced when rays touch a caustic surface produce significant waveform distortion. Calculation of these phase shifts can aid in identifying which slab models produce unrealistic waveform distortions.

Waveform complexity due to slab diffraction. In this approach it is worthwhile to compare the regional dependence of amplitudes obtained by dynamic ray tracing with the regional dependence of waveform complexity and pulse broadening obtained by methods that include the frequency

dependent effects of slab diffraction. The results of such a comparison can be used to predict the regional dependence of slab waveform effects simply on the basis of peak amplitudes. An examination of Figure 1 shows how such a prediction of slab waveform effects can be made. Note that the degree of pulse broadening and slab diffraction correlates with both amplitude and travel time anomaly. The fastest travel time and smallest amplitudes correlate with the greatest amount of pulse broadening. A 50% reduction in amplitude will begin to be associated with discernible pulse broadening. At a 70% or more reduction in amplitude, a large amount of broadening begins to be observed, often with a secondary diffracted pulse.

Calculations. The modified form of dynamic ray tracing used in this study is termed vicinity ray tracing (Kim and Cormier, 1990). The locus of a ray nearby a reference ray is calculated by integrating four differential equations for the ray centered coordinates (q_1, q_2) of the nearby ray measured from the reference ray and the angular differences (η_1, η_2) between the tangent to the reference ray and the tangent to the vicinity ray (Figure 2). These equations are

$$\frac{dq_1}{ds} = \frac{h_1^2 v}{v_1} \sin \eta_1$$

$$\frac{dq_2}{ds} = \frac{h_2^2 v}{v_2} \sin \eta_2$$

(1)

$$\begin{aligned} \frac{d\eta_1}{ds} &= \frac{h_1 v_{1,s}}{v_1} \tan \eta_1 + C \frac{v_1}{\cos \eta_1} \\ \frac{d\eta_2}{ds} &= \frac{h_2 v_{2,s}}{v_2} \tan \eta_2 + \frac{v_1}{\cos \eta_1} \end{aligned}$$

where

$$C = \frac{v, q_1}{h_1 v^2} - \frac{v v_{1,q_1} h_1^2}{v_1^3}$$

$$D = \frac{v, q_2}{h_2 v^2} - \frac{v v_{2,q_2} h_2^2}{v_2^3}$$

$$h_1 = 1 + \frac{v, 1}{v} q_1$$

$$h_2 = 1 + \frac{v, 2}{v} q_2$$

$$v = v(s, 0, 0)$$

$$v_1 = v(s, q_1, 0)$$

$$v_2 = v(s, 0, q_2)$$

Lower case v denotes velocity along the central ray and upper case V denotes velocity along a vicinity ray. Equations (1)

are integrated together with one equation for the rotation of the ray centered coordinates and the kinematic ray tracing equations in spherical coordinates.

The standard linear system of dynamic ray tracing equations can be derived from the non-linear system above if paraxial approximations are substituted. These substitutions assume q_i is small with respect to the scale length v/v_i of the medium, estimate h equal to 1, and calculate V_1 and V_2 by the first two terms of a Taylor expansion about the central ray (Kim and Cormier, 1990; Cerveny, 1985).

In this application, the primary advantage of the vicinity ray tracing equations is that amplitudes and wavefront curvature are calculated from differential equations having terms that depend on only the first spatial derivatives of velocity. Standard dynamic ray tracing requires calculation of second spatial derivatives of velocity in ray centered coordinates, involving multiple transformations between second spatial derivatives specified in ray centered, spherical, and Cartesian coordinates. While straightforward, these transformations represent significant algebraic effort in a model specified in spherical coordinates. Another advantage of the vicinity ray tracing system is that unlike standard dynamic ray tracing, in which jump conditions must be satisfied on elements of the \mathbf{Q} and \mathbf{P} matrices at discontinuities in velocity gradient, no jump conditions are

needed on (q_1, q_2) and (η_1, η_2) . Equations (1) are simply continued across first and second order discontinuities using Snell's law.

After integrating equations (1), the geometric spreading factor is calculated by

$$R = \sqrt{\frac{q_1 q_2}{\tan \eta_1 \tan \eta_2}}$$

(2)

$\pi/2$ phase changes are tracked along the reference ray by counting the number of sign changes in q_1 and q_2 as equations (1) are integrated. The amplitude of a body wave at any point along the reference ray is proportional to $1/R$. In the examples discussed in the following sections, amplitudes and travel times are displayed as contoured residual spheres (Creager and Jordan, 1984) of travel times and amplitudes anomalies computed in a reference radially symmetric model PREM (Dziewonski and Anderson, 1981) and PREM perturbed by a slab structure. The travel time residuals are computed from $T_0 - T_S$ and the amplitude residuals from $\log_{10} A_0 - \log_{10} A_S$, where the subscript o denotes the result for the reference model and the subscript S denotes the result for the perturbed model.

Slab parameterization. Most of the slab velocity models are derived from thermal models specified on two-dimensional

grids. The two-dimensional Cartesian grids are converted to a polar grids using a transformation between angular θ and horizontal X distance, $\theta = X/r$ where r is the radius corresponding to the mid-depth point of the thermal model. The thermal models are next converted to velocity models by assuming a temperature derivative of velocity. All models extend $\pm 5^\circ$ along strike from the assumed source position. The slab models are added as perturbations to a radially symmetric model, taken to be the 1 Hz. isotropic PREM (Dziewonski and Anderson, 1981). Within the slab, the fractional perturbation of S velocity from its value in the surrounding mantle is observed to be more than twice the fractional perturbation of P velocity, or $\delta\beta/\beta \geq 2 \delta\alpha/\alpha$. For values of $\delta\ln\beta/\delta\ln\alpha \geq \alpha/\beta$ (about 1.7 in the mantle) perturbations of ray paths will be larger for S waves than P waves, and the effects of slab structure are expected to be larger on S than on P waves. Hence, many studies, including the one presented in this paper, concentrate on modeling slab effects on shear waves.

Focusing and Defocusing Experiments

Slab Distortion Below 650 km Depth?

Vicinity ray tracing was performed for a series of different slab models derived from thermal models with varying source

locations and a temperature derivatives of S velocity, $d\beta/dT = 0.65 \text{ m s}^{-1} \text{ K}^{-1}$. The first two models considered were derived from P velocity models proposed by Creager and Jordan (1986) and Fischer et al. (1988) for the Kuril-Kamchatka slab. For this slab, Fischer et al. examined the tradeoffs in slab width, penetration, and velocity perturbation below 650 km depth consistent with P travel time residuals. Figure 3 shows the form of the two models, A and B, which cannot be distinguished at similar high confidence levels by travel time inversion. Model A, which remains thin below 650 km depth, was slightly better than Model B in reducing the variance calculated from difference between observed and predicted P residuals.

Figure 4 compares the S and ScS travel time residuals derived from the P wave models under the assumption that $d\beta/dT = 0.65 \text{ m s}^{-1} \text{ K}^{-1}$. These travel time residuals, as well as all others shown in this paper, have a mean value averaged over area added to the true residual pattern, which is uniformly negative. The addition of the mean value or choice of a zero baseline is designed to mimic the processes of residual sphere smoothing and correction for an unknown origin time described in Creager and Jordan (1984). Although significantly larger negative anomalies in S and ScS travel time are observed in the model B, which thickens below 650 km depth, it might be difficult to distinguish between A and B using P data having a 3.5 factor smaller gain in anomaly.

The smallest P anomalies would be swamped by noise in the data, and it would require a dense azimuthal coverage in regions having the strongest anomalies to discriminate between the two models. Both models A and B predict maximum anomalies in ScS travel times roughly consistent with those first reported by Jordan (1977). Model B appears to be in slightly better agreement with Jordan's (1977) ScS data for the Kuril-Kamchatka slab, coming closer to the peak ScS travel time anomalies of about -7 seconds.

Figure 5 compares the S and ScS amplitude anomaly predicted for the two models shown in Figure 3. The amplitude anomalies in Figure 5 correlate with the travel time anomalies in Figure 4 only in a broad regional sense. In model A, the lowest amplitudes and fastest travel times are located on the dipping side of the slab in azimuthal sectors centered about lines at $\pm 15^\circ$ with respect to the strike of the slab. In model B the most intense anomalies are aligned closer to the strike of the slab. The broad sense of the correlation of amplitudes and travel times in these regions agrees with the expectation that a high velocity region such a descending slab will defocus body waves. The lowest amplitude anomaly of model A is -0.9 and the minimum travel time anomaly is -5 seconds; for model B it is -0.8 in amplitude and -10 seconds in travel time anomaly. In both models, the minimum amplitude anomaly is displaced in position from the minimum travel time anomaly. Note, for

example, that the minimum amplitude anomaly in model B will occur at 40 to 50 great circle degrees at azimuths close to the strike of the slab, whereas the minimum travel time anomaly will occur around 70 great circle degrees at azimuths displaced slightly toward the side of the slab opposite its dip. At azimuths perpendicular to the strike on the dipping side of the slab, zero and weak positive S amplitude anomalies are associated with weak positive and negative S travel time anomalies. There are thus many local exceptions to the expected rule of fast regions correlating with regions of low amplitude and slow regions correlating with regions of large amplitudes.

These results agree with the results obtained by Weber (1990) in a two-dimensional study of slab focusing and defocusing. They also illustrate that amplitudes can provide constraints independent of travel times in the modeling of slab structure. A similar result has been more rigorously demonstrated in studies that attempt to invert for structure, simultaneously using amplitude and travel time data. Nowack and Lutter (1988) have shown that amplitudes are most sensitive to the edges of a velocity anomaly, while travel times are most sensitive to the center of a velocity anomaly. This effect can be most clearly seen in plots of ray trajectory, in which rays shot at equal take off angles are often seen to concentrate in regions of strong velocity gradient (e.g., Cormier and Spudich, 1984; Cormier, 1987).

From these results, we can expect that amplitude data may be potentially valuable in resolving the boundaries of a slab structure and its total width.

In Figure 5, both A and B models predict large negative amplitude anomalies (defocusing) of S waves observed along the strike of the slab. The regions in which the negative anomaly in log amplitudes is less than -0.5 can be expected to exhibit a significant amount of pulse broadening due to slab diffraction. Model A, which remains thin below 650 km depth, defocuses ScS as well as S along the strike of the slab. Model B, which thickens below 650 km depth, however, defocuses ScS to a much lesser extent. Using Figure 1 to predict slab diffraction effects, one can conclude that model A, which remains thin below 650 km, will broaden the waveform of both S and ScS along strike, whereas model B, which thickens below 650 km, will broaden S but not ScS along strike. The broadening of ScS in model A will cover nearly an entire 180° sector on the dipping side of the slab. The broadening of S in model B will be concentrated in geographic regions along azimuths parallel to the strike of the slab at distances less than about 60° .

Broadband S and ScS waveforms from deep focus Kuril-Kamchatka events can be observed at azimuths along the strike of the slab at seismographic stations in North America (Silver and Chan, 1986). Since in most of the examples collected, it is

S and not ScS that seems to have significantly broader pulse width, these data are most consistent with a Kuril-Kamchatka slab that advectively thickens below 650 km depth.

A similar conclusion was reached in the S waveform studies of Vidale (1987), using a two-dimensional finite difference synthesis method, and by Cormier (1989), using a superposition of Gaussian beams in two and three dimensions. These studies concluded that while some deep slab structure may be present below 650 km depth, an S velocity model of type A, which remains thin below 650 km depth, predicts too large a distortion in the waveforms of S waves at take-off angles corresponding to ScS and SKS. In our present study, assuming the correctness of the hypothesis that strong amplitude anomalies are associated with pulse broadening, a slightly stronger conclusion can be made. Not only is Model A inconsistent with the observed S waveform data, but features of Model B, having some advective thickening below 650 km depth, may begin to predict some of the trends seen in the data, i.e., the strongest pulse broadening is observed along strike in S waves at distances equal to or less than 55 degrees (Figure 6).

Gaherty et al. (1989) have compared SH and ScSH amplitude and travel time residuals for several deep focus earthquakes occurring in the Kuril-Kamchatka slab. A signature of slab structure in their data can primarily be seen in azimuths

along strike. When compared with predicted amplitude anomalies, the observed amplitude anomalies seem to be more consistent with a slab that has grown in width below 650 km depth than one that has remained thin below that depth. A thin deeply penetrating slab predicts much stronger than observed amplitude and travel time anomalies along azimuths perpendicular to the strike in the down dip direction.

*Effect of a Discontinuous Increase in Mantle Viscosity at
650 km Depth*

The two slab models just discussed have been based on thermal models that do not account for variations in the viscosity of the mantle and the temperature dependence of viscosity. Advective thickening was introduced in an ad hoc fashion to investigate the range of possible models consistent with travel time anomalies.

Gurnis and Hager (1988) have computed a thermal model that includes the effects of a lower mantle having a factor of 30 increase in viscosity. The effect of the viscosity increase is to induce advective thickening in the thermal structure and a pronounced broadening of the slab velocity anomaly below 650 km depth, with much a much weaker thermal anomaly

and inferred velocity anomalies below 650 km than in Model B (Figure 7).

The predicted amplitude and travel time anomalies of S and ScS waves for a 540 km deep earthquake are shown in Figure 8. Measurable travel time and amplitude anomalies are seen primarily in the S waves and less so in ScS waves for deep focus sources. The gain in the travel time anomalies is roughly equivalent to that of Model A for the Kuril-Kamchatka slab, but the gain in amplitude anomalies is much weaker than either models A and B and the location of the peak anomalies in both travel time and amplitude has been shifted to shorter distance ranges in S. Using the waveforms shown in Figure 1 to calibrate the amplitude and anomalies for waveform broadening, it is predicted that the Gurnis and Hager model will not produce much waveform distortion in either the S or ScS waves of deep focus earthquakes, except possibly in S waves at ranges between 40 to 60 degrees at azimuths 10 to 30 degrees from the strike of the slab on dipping side of the slab.

Comparison of the amplitude anomalies shown in Figure 8 with the pulse broadening data shown in Figures 6 suggests that model B is a better model for the Kuril-Kamchatka slab. Even if the dip of the Gurnis and Hager model were steepened to be consistent with the dip of the Benioff zone defining the Kuril-Kamchatka slab, it would produce too small of an

amplitude anomaly in S to be consistent with the waveform broadening observed reported by Silver and Chan (1986) at azimuths along the strike of the slab. The intensity of travel time anomalies in ScS observed from deep focus events in the Kuril-Kamchatka slab (Jordan, 1977) is also more consistent with the stronger intensity of S velocity anomaly below 650 km depth shown in Figure 3b.

Variations in Source Position

With the best data available for hypocentral location, including travel times from local arrays above the earthquake and/or calibration of local structure from a master event, it is never possible to locate the hypocenter of a deep focus event to any accuracy better than about ± 10 km. In practice, this lower limit is also set by the characteristic source dimension of the $m_b = 5.5$ to 6 of deep focus earthquakes most commonly studied at teleseismic range. It is generally unknown whether most of the energy observed in a body wave or teleseismic range is radiated at or near the point at which rupture initiated or stopped. Although it may be reasonable to assume that rupture initiates in the highest velocity core of the slab, this is as yet an unproved assumption. For these reasons, it is important to investigate the effect of source position within a slab on the pattern of amplitude and travel time anomalies.

The amplitudes and travel times of S and ScS waves were calculated for a SH point source located at positions I to V in the slab model shown in Figure 9. Figure 10 shows the resultant travel time and amplitude anomaly patterns for lateral positions I and II.

The results of these tests can be summarized as follows:

1. *Lateral position fixed and depth varied.* Amplitudes and travel times smoothly change, with anomalies decreasing in amplitude as source depth increases.
2. *Fixed source position and temperature derivative of velocity varied.* Amplitudes and travel times smoothly change, with anomalies decreasing in magnitude as temperature derivative of velocity decreases.
3. *Depth fixed and lateral position varied.* For changes in lateral position up to 50 km, broad regional anomalies in amplitude and travel times change by a small amount, but transitions between low and high amplitudes or between fast and slow times change dramatically in location and intensity. Figure 11 compares the end points of S rays for source positions I and II, showing that multipathing and caustics are easily induced when the lateral location is near a rapid change in velocity gradient. There are some features in the anomaly pattern that are relatively stable for changes in

lateral source position, e.g., the broad anomaly in S waves in the down dip direction at azimuths close to the strike of the slab and the strong anomalies in ScS everywhere on the dipping side of the slab.

For purposes of using amplitudes to model slab structure, the most important of these is the third result. The broad amplitude low and travel time minimum in S waves on the down dip side of the of the slab at azimuths close to the strike and the strong anomalies in ScS everywhere on the dipping side of the slab are the most stable features of the anomaly pattern of a thin, deeply penetrating slab. These features are relatively insensitive to changes in source position up to 50 km vertically or laterally. Their presence or absence and their intensity strongly constrain the slab structure below the hypocenter. If the intensity of the amplitude anomaly is less than -0.5 in log amplitude units than it is likely also to be associated with a secondary, slab diffracted pulse and/or broadening. If strong amplitude and/or waveform anomalies are absent in ScS but are present in S primarily along azimuths close to the strike of the slab, then such an observation would suggest slab penetration below below the hypocenter but with some distortion and advective thickening.

Bent Slabs and Multipathing

Multipathing in three-dimensional structure, as in two-dimensional structure, is usually associated with the development of caustic surfaces and Hilbert transformation of ray paths that touch the caustic surfaces. Silver and Chan (1986) suggested that multipathing may be responsible for the pulse broadening observed in some of the broad band S waveforms they observed from deep focus events. To explain the observed waveforms, the multipathing must be such that the interfering multiples produce displacement pulses that do not change polarity throughout the summed waveforms of the multiples. Since the $\pi/2$ phase shift of the Hilbert transformation produces time segments of both positive and negative polarities, the multipathing scenarios proposed by Silver and Chan were investigated to see if they can produce broadened displacement waveforms of constant apparent polarity.

Silver and Chan found that bent slabs such as that shown in Figure 12 can produce multipathing in several different azimuthal regions for sources that lie in the region above the bend. Figure 13 shows that two types of azimuthal regions will exhibit multipathing. Figure 14 shows waveforms predicted from vicinity ray tracing to receivers

anomalies. Ray tracing experiments show that this behavior is consistent with amplitudes being most sensitive to the edges of a velocity anomaly, while travel times are most sensitive to the center of a velocity anomaly.

Use of Waveforms and Amplitudes in Modeling Slab Structure.

Waveforms and amplitudes provide independent constraints in the modeling of slab structure. The relative broadening and amplitude anomalies of direct S versus those of S waves having steep vertical take-off angles, such as ScS and SKS, are particularly valuable in discriminating between different slab structures below 650 km depth. Although waveforms, amplitudes, and travel times vary most rapidly in the azimuthal region surrounding the strike of the slab, a dense sample of S and ScS waveforms in this region can provide powerful constraints on deep slab structure. Waveform broadening in S but not ScS from deep focus earthquakes observed along the strike of the slab, for example, is consistent with advective thickening and slab distortion below 650 km depth.

The Kuril-Kamchatka Slab

Strong negative anomalies in the travel times of ScS waves at azimuths on the dipping side of the slab and waveform

broadening in S waves at azimuths along the strike of the slab from the deepest focus earthquakes strongly argue for some type of slab structure or thermal anomaly below 650 km depth. Thin, deeply penetrating slabs, however, produce strong signatures in the amplitudes and waveforms of ScS, SKS, and SKKS in a broad azimuthal range on the dipping side of the slab that are not observed in data. Waveform broadening in S but not ScS at ranges less than 60° at stations along the strike of the slab suggests either a decrease in the temperature contrast of the slab, a decrease in the temperature derivative of S velocity ($d\beta/dT$) and/or some advective thickening or distortion below 650 km depth. A model of the Kuril-Kamchatka data most consistent with all data is one in which a slab structure exists below 650 km depth, but with a factor two to three advective thickening over the deep slab models originally proposed by Creager and Jordan (1986).

Acknowledgements. We thank M. Weber, J. Gaherty, and T. Lay for reprints of their work prior to publication. Figures were prepared with the help of Wei-jou Su. This research was supported by the National Science Foundation under grant EAR 89-04236 and by the Advanced Research Projects Agency of the Department of Defense, monitored by the Geophysics Laboratory under contract F19628-88-K-0010.

References

- Cerveny, V., The application of ray tracing to the propagation of shear waves in complex media, in *Seismic Exploration*, edited by S. Treitel and K. Helbig, Geophysical Press, London, pp. 1-124, 1985.
- Cormier, V.F., and P. Spudich, Amplification of ground motion and waveform complexity in fault zones: examples from the San Andreas and Calaveras faults, *Geophys. J. R. Astr. Soc.*, 79, 135-153, 1984.
- Cormier, V.F., Focusing and defocusing of teleseismic P waves by known three-dimensional structure beneath Pahute Mes Mesa Nevada Test Site, *Bull Seismol Soc. Am.*, 77, 1688-1703, 1987.
- Cormier, V.F., Slab diffraction of S waves, *J. Geophys. Res.*, 94, 3006-3024, 1989.
- Creager, K.C., and T.H. Jordan, Slab penetration into the lower mantle, *J. Geophys. Res.*, 89, 3031-3049, 1984.
- Creager, K.C., and T.H. Jordan, Slab penetration into the lower mantle beneath Mariana and other island arcs of the north Pacific, *J. Geophys. Res.*, 91, 3573-3590, 1986.
- Davies, D., and B.R. Julian, A study of short period P wave signals from Longshot, *Geophys. J. R. Astron. Soc.*, 29, 185-202, 1972.
- Dziewonski, A.M., and D.L. Anderson, Preliminary reference Earth model, *Phys. Earth Planet Inter.*, 25, 297-356, 1981.
- Engdahl, E.R., J.E. Vidale, and V.F. Cormier, Wave propagation in subducted lithospheric slabs, in *Proceedings of the 6th Course: Digital Seismology and Fine Modeling of the Lithosphere, International School of Applied Geophysics, Majorana Center, Erice, Sicily, Plenum, New York*, 1989.
- Fischer, K.M., T.H. Jordan, and K.C. Creager, Seismic constraints on the morphology of deep slabs, *J. Geophys. Res.*, 93, 4773-4783, 1988.
- Gaherty, J., T. Lay, and J. Vidale, Constraints on deep slab structure from shear waveform analysis, (abstract) *EOS Trans. Am. Geophys. Un.* 70., 1989.

- Gurnis, M., and B.H. Hager, Controls on the structure of subducted slabs, *Nature*, 335, 317-321, 1988.
- Jordan, T.H., Lithospheric slab penetration into the lower mantle beneath the Sea of Okhotsk, *J. Geophys.*, 43, 473-496, 1977.
- Kim, W., and V.F. Cormier, Vicinity ray tracing: an alternative to dynamic ray tracing, *Geophys. J. Int.*, in press, 1990.
- Nowack, R.L., and W.J. Lutter, Linearized rays amplitudes and nversion, 401, 421, 1988.
- Sleep, N.H., Teleseismic P-wave transmission through slabs, *Bull. Seism. Soc. Am.*, 63, 1349-1373, 1973.
- Silver, P.G., and W.W. Chan, Observations of body-wave multipathing from broad-band seismograms: Evidence for lower mantle slab penetration beneath the Sea of Okhotsk, *J. Geophys. Res.*, 91, 3,787-13,802, 1986.
- Vidale, J.E., Waveform effects of a high-velocity, subducted slab, *Geophys. Res. Lett.*, 14, 542-545, 1987.
- Vidale, J.E., and D. Garcia-Gonzalez, Seismic observation of a high velocity slab 1200-1600 km in depth, *Geophys. Res. Lett.*, 15, 369-372, 1988.
- Weber, M., Subduction zones -- their influence on traveltimes and amplitudes of seismic signals, *Geophys. J. Int.*, in press, 1990.
- Witte, D., PhD. Thesis, Columbia University, 1987.

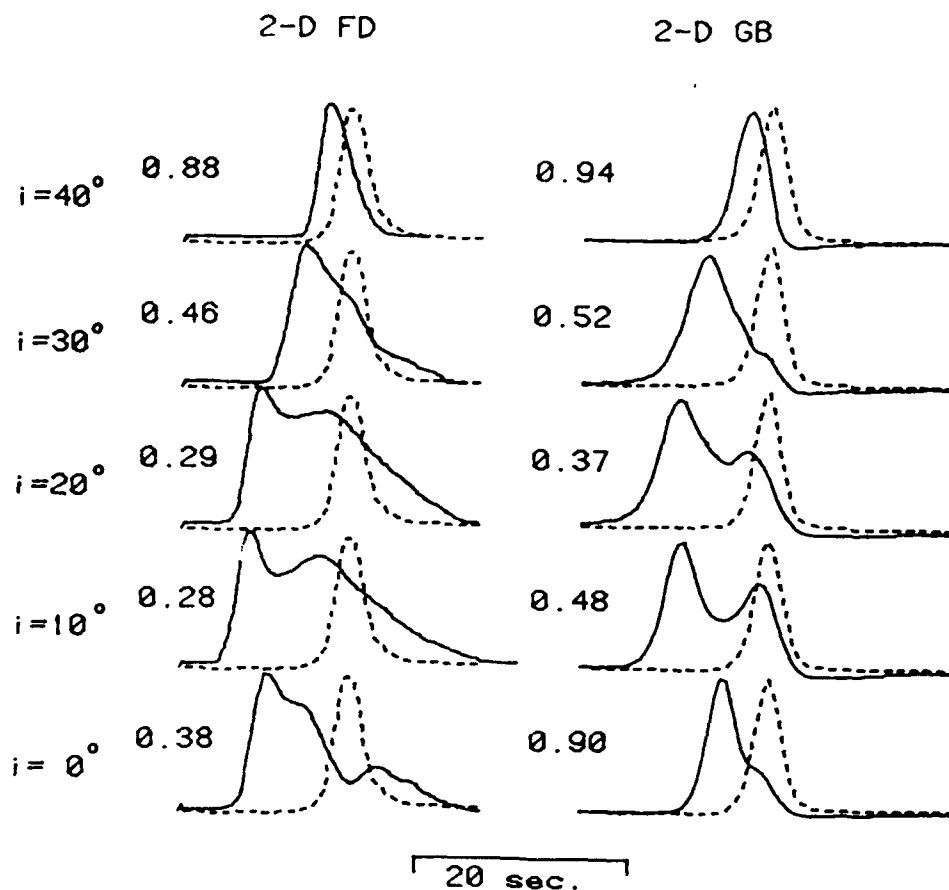


Figure 1. SH waves radiated by a deep focus point source in a slab model synthesized by the two-dimensional a finite difference calculation (Vidale, 1987) and a three-dimensional superposition of Gaussian beams shot reciprocally from receiver to source (Cormier, 1989). The dashed traces are reference waveforms for PREM patched to a homogeneous halfspace at 1400 km depth. Numbers to the left of each trace give the ratio of the peak amplitude of the seismograms synthesized in the slab structure to the peak amplitude of the reference waveforms.

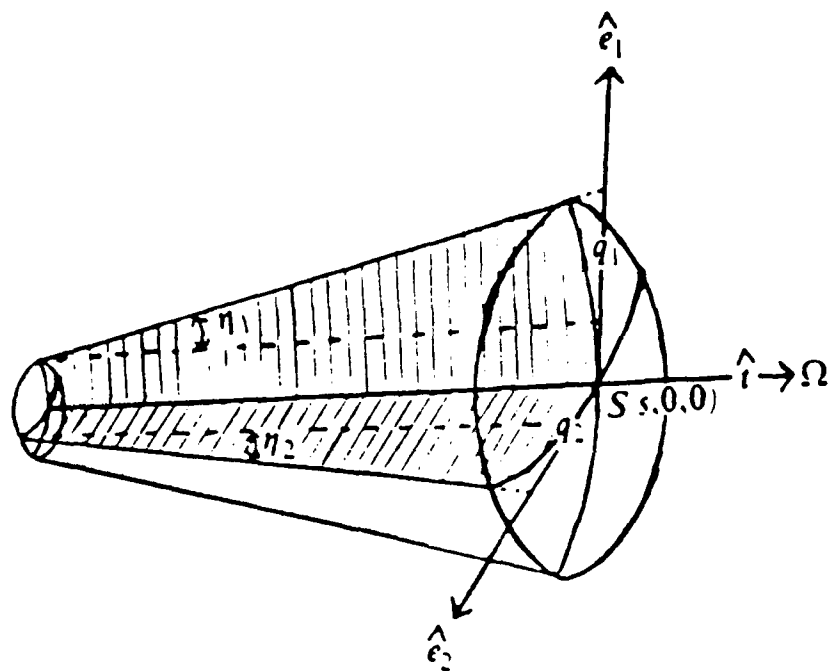
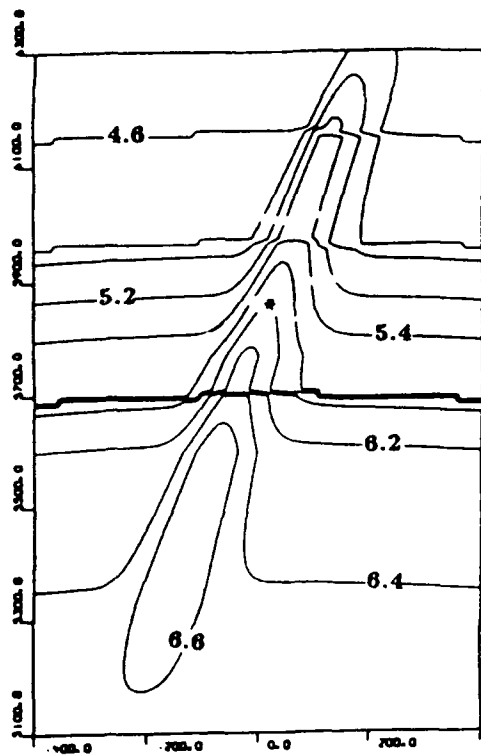


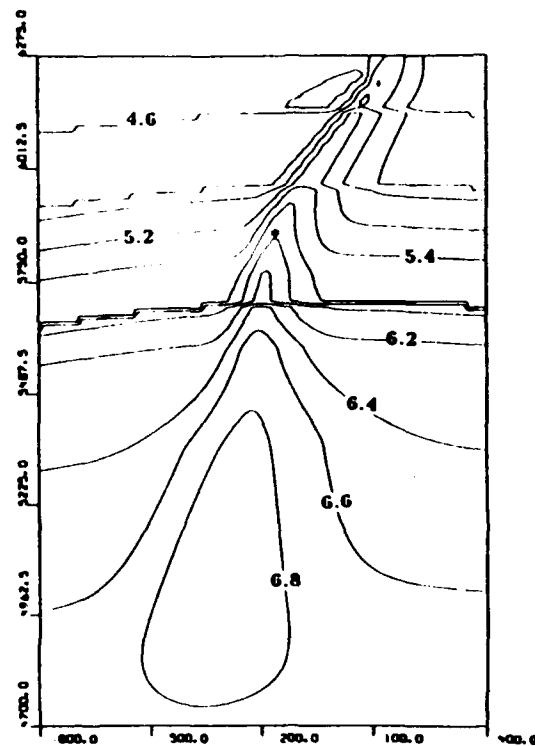
Figure 2. Geometry and definition of the quantities η_i and q_i in the vicinity ray tracing system.

I. Narrow Slab Below 650 km. -- Kurils



(a)

II. Wide Slab Below 650 km. -- Kurils



(b)

Figure 3. S wave models of the Kuril-Kamchatka slab based on thermal models determined from P wave travel time anomalies in studies by (a) Creager and Jordan (1986) and (b) Fischer et al. (1988). Model (b) is the end member of a series of models consistent with the data having the greatest amount of advective thickening beneath 650 km.

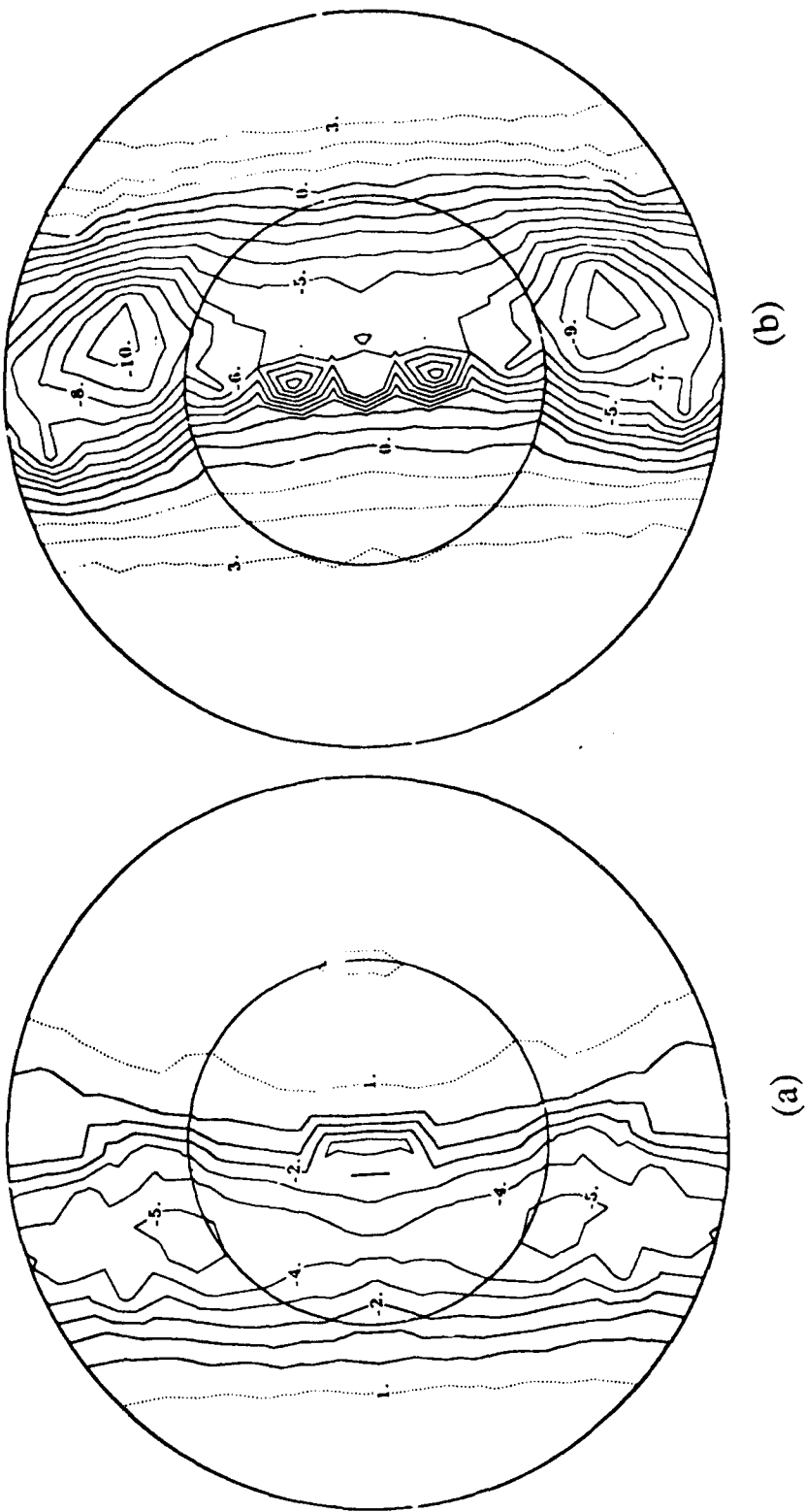


Figure 4. Comparison of travel time anomalies in slab models (a) and (b) shown in Figure 3.

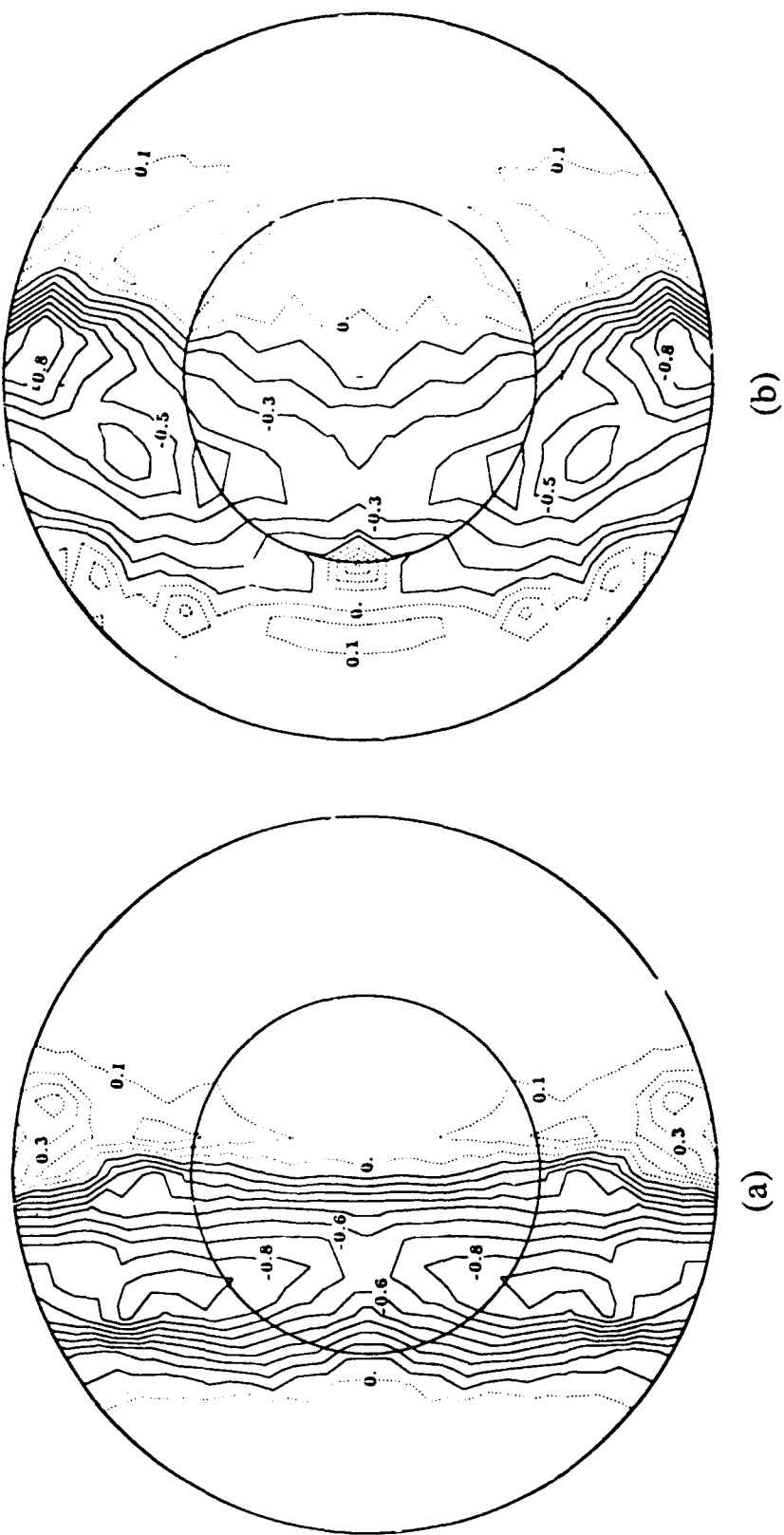


Figure 5. Comparison of amplitude anomalies in slab models (a) and (b) shown in Figure 3.

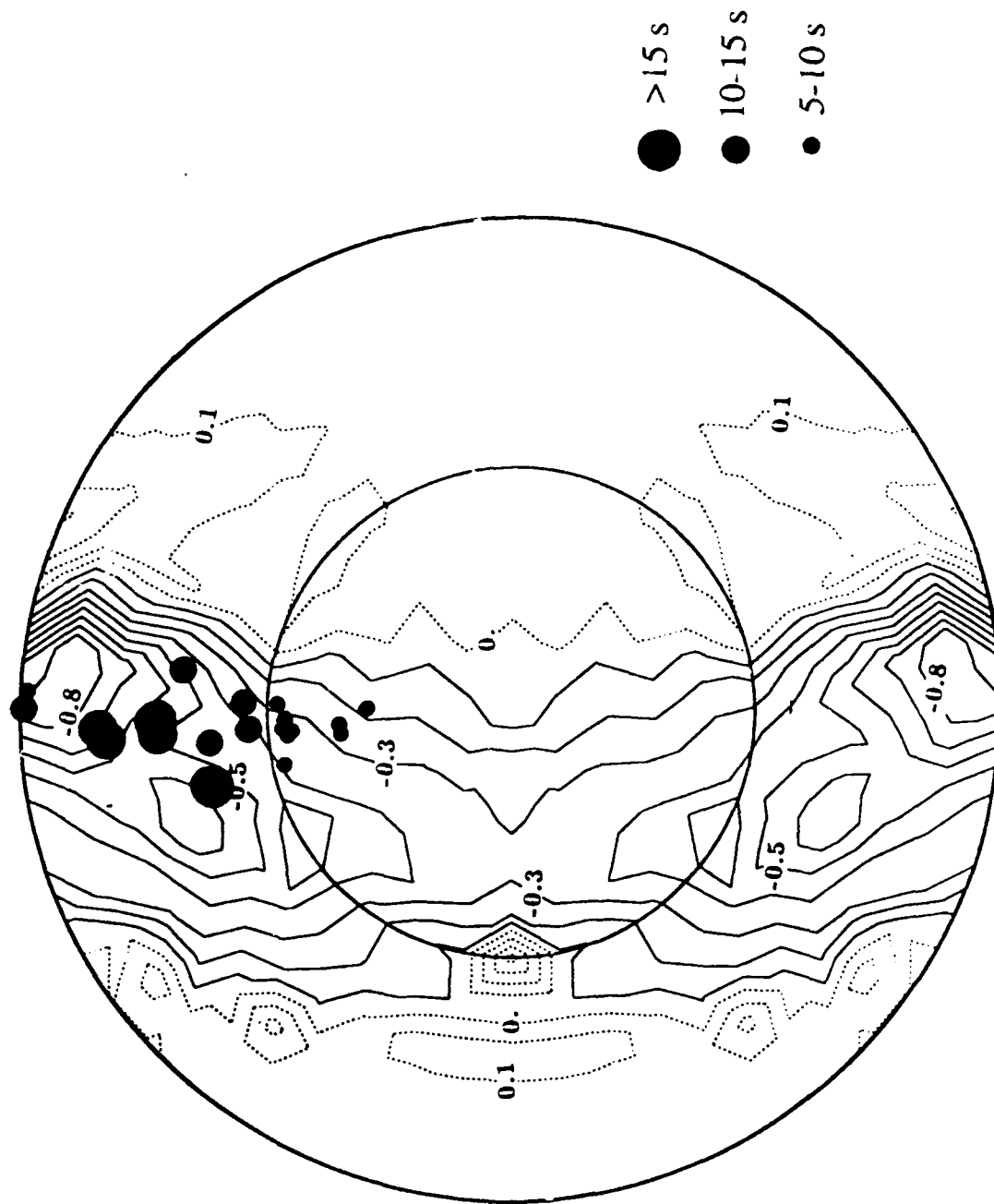


Figure 6. Pulse broadening of S and ScS in seconds calculated by Silver and Chan (1986) from two deep focus earthquakes in the Kuril-Kamchatka slab. Pulse broadening anomalies are plotted in the contoured residual spheres of peak amplitude anomalies of slab model (b) of Fischer et al. (1988).

**Wide Slab Below 650 km.
(Effect of Viscosity Increase at 650 km.)**

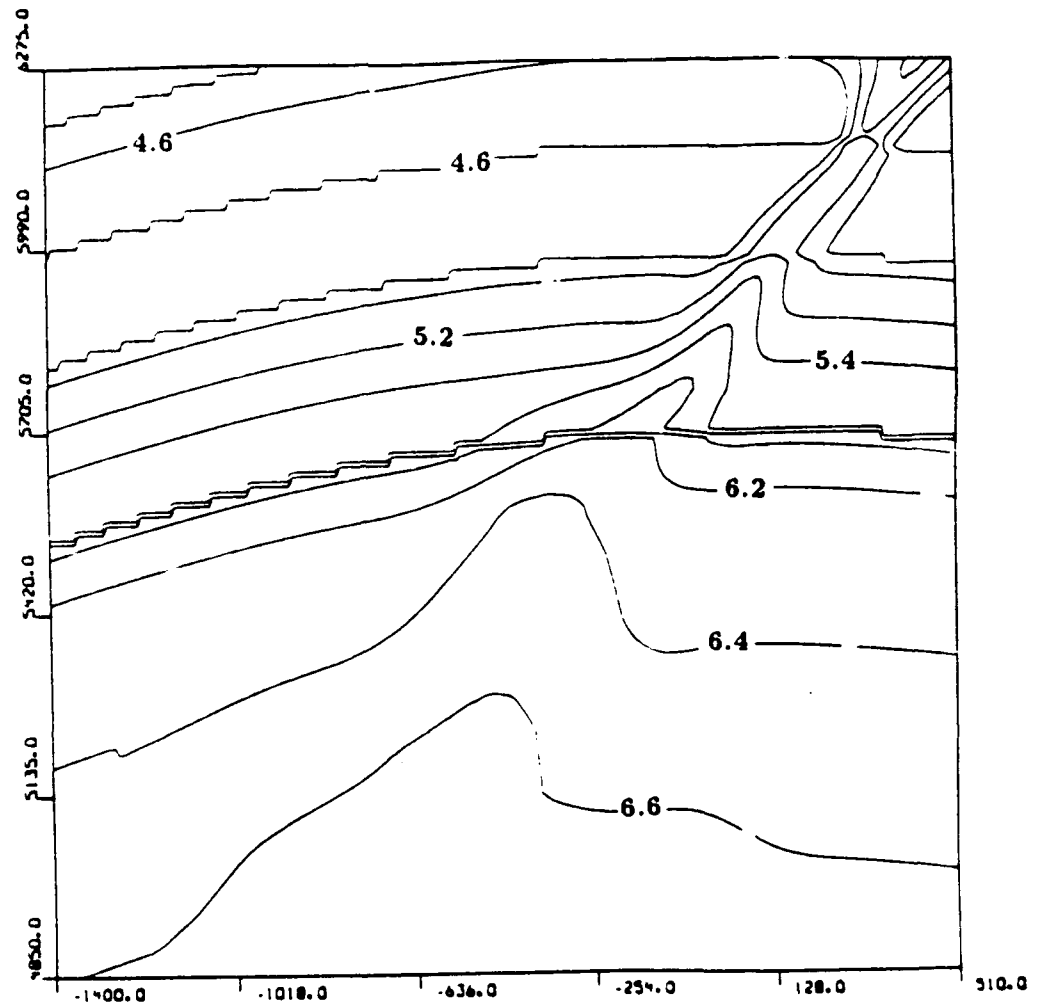
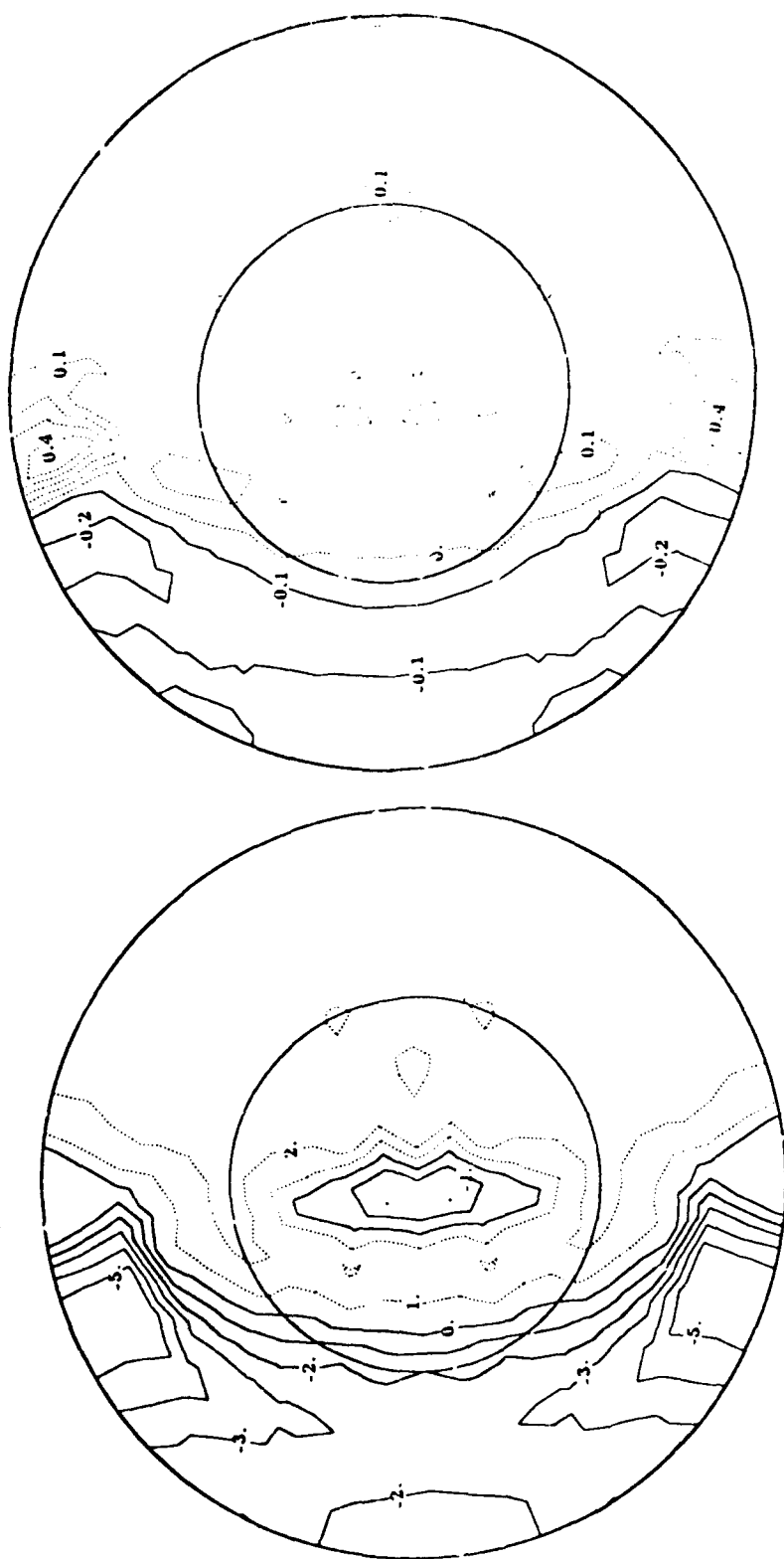


Figure 7. Slab model for S velocity determined from the thermal model of Gurnis and Hager (1988) for a slab encountering a factor 30 increase in viscosity at 650 km depth.



GURNIS AND HAGER MODEL

S Travel Time Anomalies

S Amplitude Anomalies

Figure 8. Travel time and amplitude anomalies computed for the slab model shown in Figure 7.

Effect of Source Location

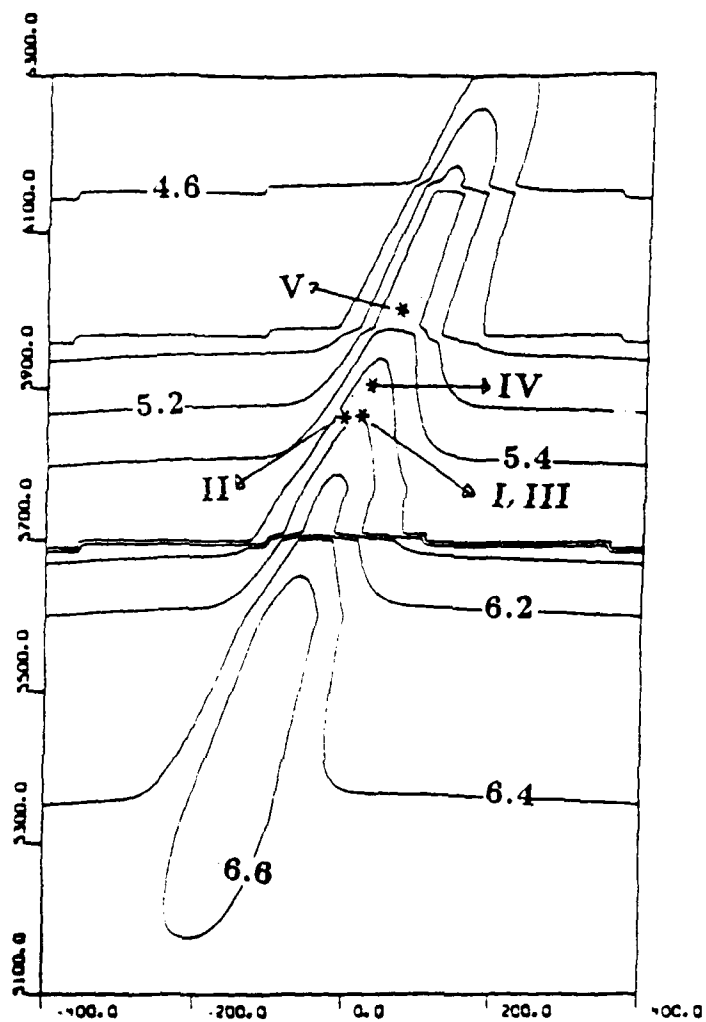
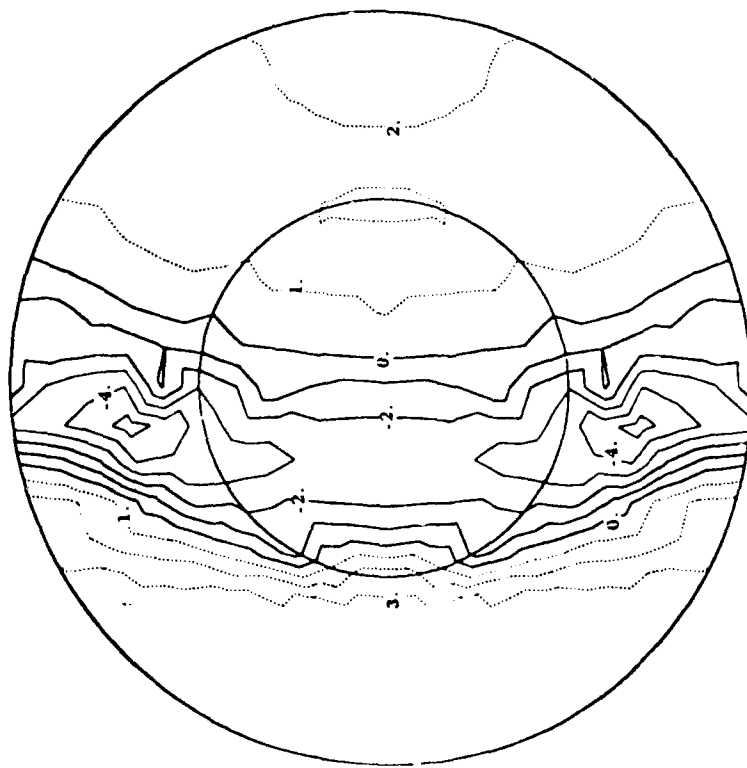
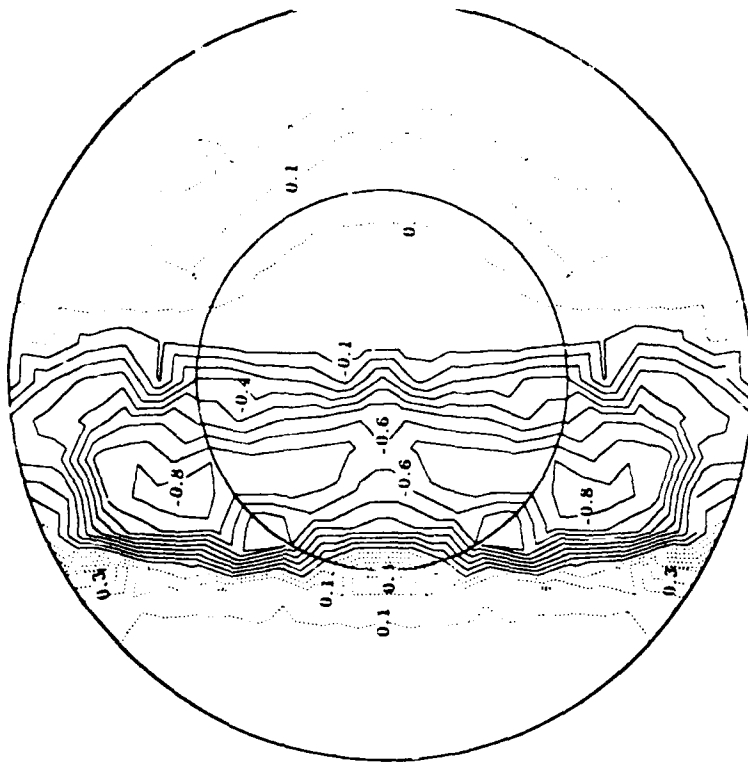


Figure 9. Source positions used in experiments to determine the effects of unknown source position on amplitude anomalies.



S Travel Time Anomalies



S Amplitude Anomalies

Figure 10. Travel time and amplitude anomalies for a shift in lateral source position toward the region of high velocity gradient defining the upper surface of the slab. These can be compared with the anomalies computed for a source position in the center of the high velocity core in Figures 4a and 5a.

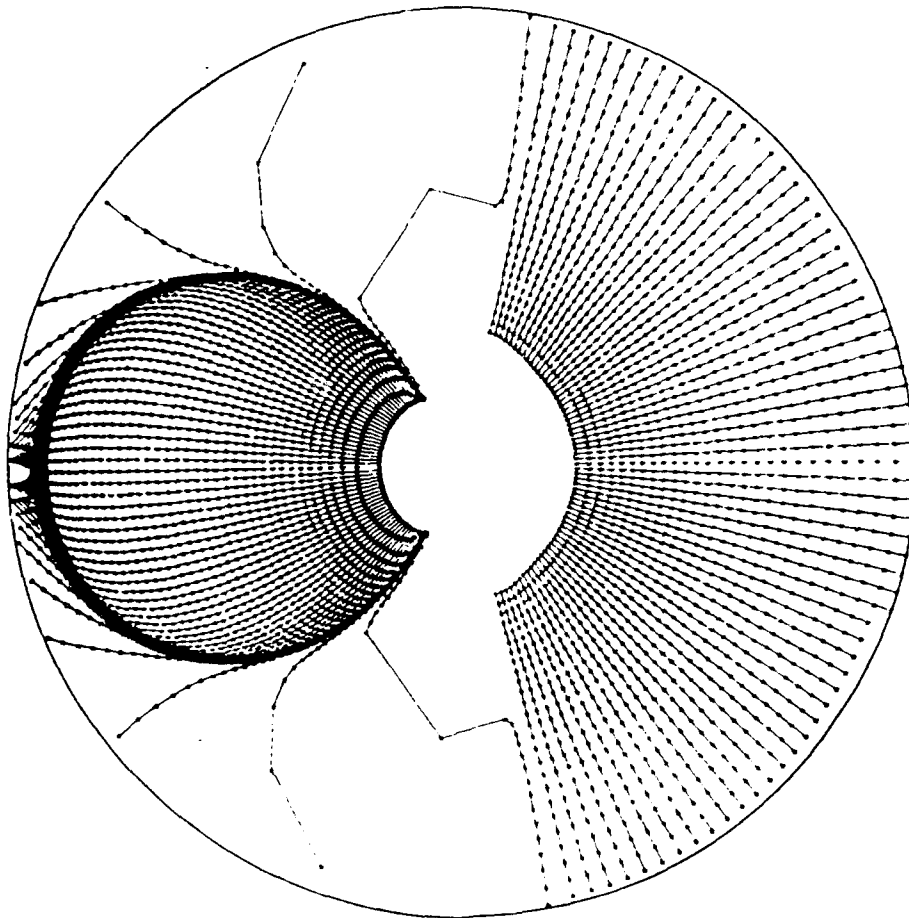


Figure 11. Ray end points projected onto an equal area geographic map for SH waves radiated by the laterally shifted source position II shown in Figure 9. End points are connected for constant azimuthal take-off angles and variable vertical take-off angle.

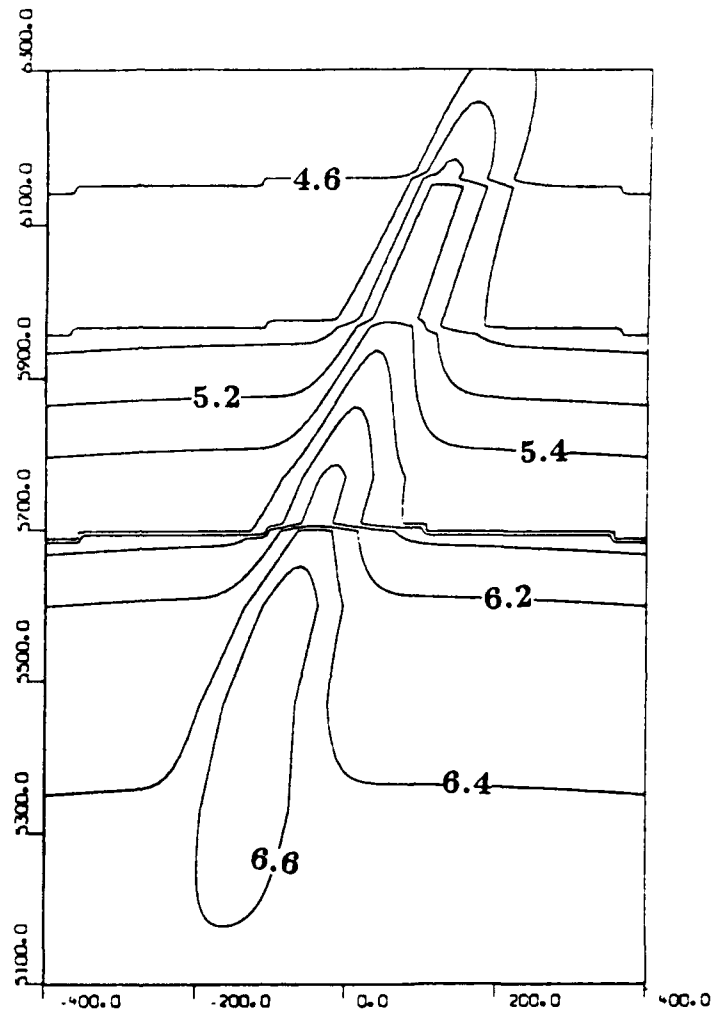


Figure 12. A bent slab model of the type considered by Silver and Chan (1986) for the Kuril-Kamchatka slab. Amplitudes, travel times, and SH waveforms are calculated for the source location shown.

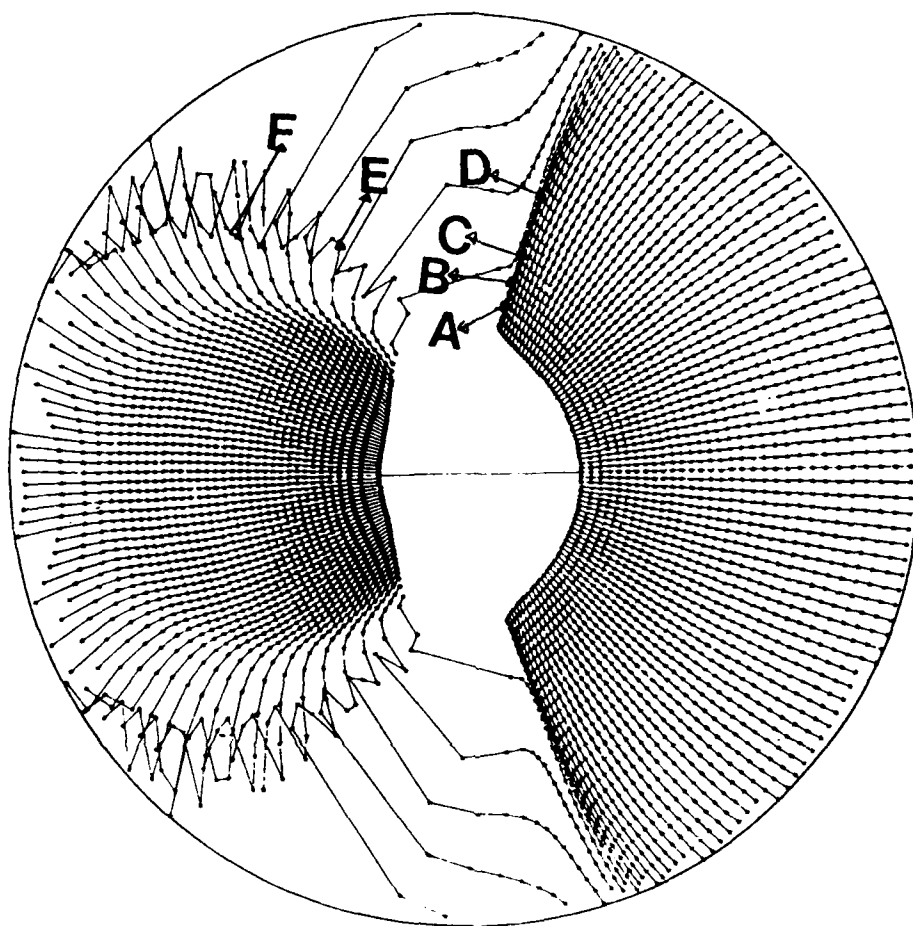


Figure 13. Ray end points projected onto an equal area geographic map for SH waves radiated by the source located as shown in Figure 12. End points are connected for constant azimuthal take-off angles and variable vertical take-off angle, illustrating two types of multipathing. Seismograms were synthesized at geographic locations A - D by summing pulses from each multipath, including effects of the Hilbert transformation.

SH-Synthetic Seismograms for Example X

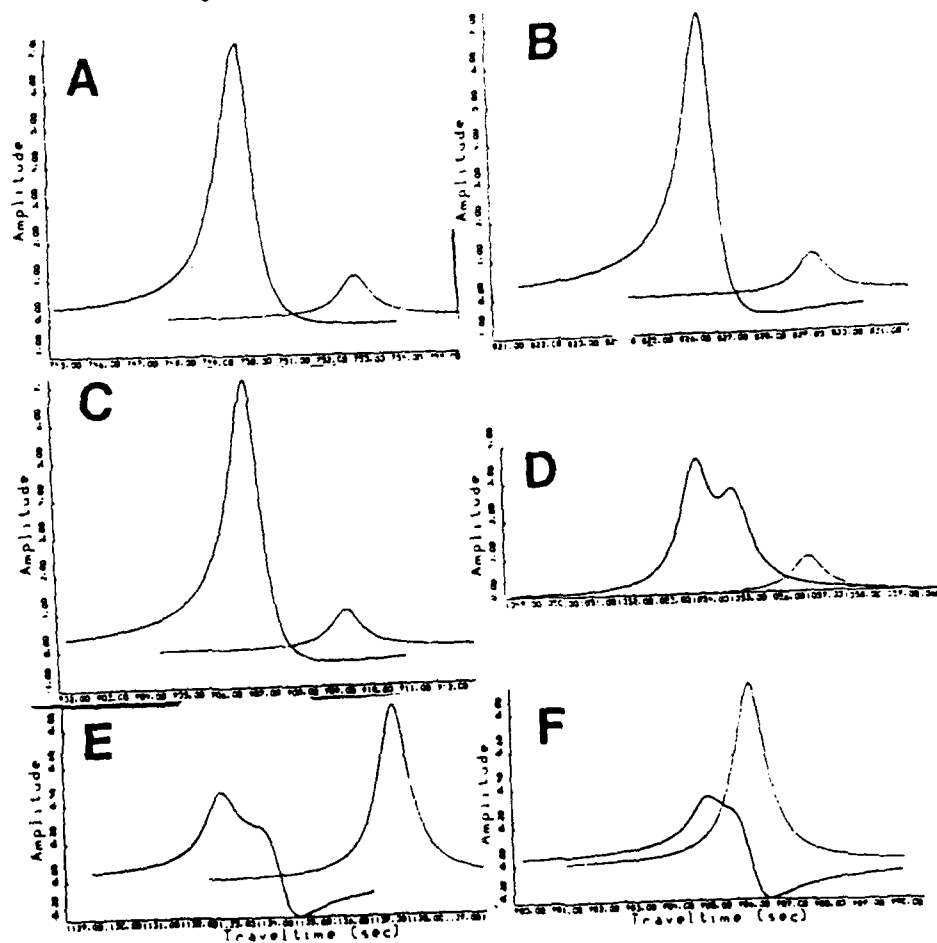


Figure 14. Synthetic SH waveforms at locations A-D shown in Figure 13. Source radiation pattern is assumed constant and effects of intrinsic attenuation are not included.

Prof. Thomas Ahrens
Seismological Lab, 252-21
Division of Geological & Planetary Sciences
California Institute of Technology
Pasadena, CA 91125

Prof. Charles B. Archambeau
CIRES
University of Colorado
Boulder, CO 80309

Dr. Thomas C. Bache, Jr.
Science Applications Int'l Corp.
10260 Campus Point Drive
San Diego, CA 92121 (2 copies)

Prof. Muawia Barazangi
Institute for the Study of the Continents
Cornell University
Ithaca, NY 14853

Dr. Douglas R. Baumgardt
ENSCO, Inc
5400 Port Royal Road
Springfield, VA 22151-2388

Prof. Jonathan Berger
IGPP, A-025
Scripps Institution of Oceanography
University of California, San Diego
La Jolla, CA 92093

Dr. Lawrence J. Burdick
Woodward-Clyde Consultants
566 El Dorado Street
Pasadena, CA 91109-3245

Dr. Karl Coyner
New England Research, Inc.
76 Olcott Drive
White River Junction, VT 05001

Prof. Vernon F. Cormier
Department of Geology & Geophysics
U-45, Room 207
The University of Connecticut
Storrs, CT 06268

Professor Anton W. Dainty
Earth Resources Laboratory
Massachusetts Institute of Technology
42 Carleton Street
Cambridge, MA 02142

Prof. Steven Day
Department of Geological Sciences
San Diego State University
San Diego, CA 92182

Dr. Zoltan A. Der
ENSCO, Inc.
5400 Port Royal Road
Springfield, VA 22151-2388

Prof. John Ferguson
Center for Lithospheric Studies
The University of Texas at Dallas
P.O. Box 830688
Richardson, TX 75083-0688

Prof. Stanley Flatte
Applied Sciences Building
University of California
Santa Cruz, CA 95064

Dr. Alexander Florence
SRI International
333 Ravenswood Avenue
Menlo Park, CA 94025-3493

Prof. Stephen Grand
University of Texas at Austin
Department of Geological Sciences
Austin, TX 78713-7909

Prof. Henry L. Gray
Vice Provost and Dean
Department of Statistical Sciences
Southern Methodist University
Dallas, TX 75275

Dr. Indra Gupta
Teledyne Geotech
314 Montgomery Street
Alexandria, VA 22314

Prof. David G. Harkrider
Seismological Laboratory
Division of Geological & Planetary Sciences
California Institute of Technology
Pasadena, CA 91125

Prof. Donald V. Helmberger
Seismological Laboratory
Division of Geological & Planetary Sciences
California Institute of Technology
Pasadena, CA 91125

Prof. Eugene Herrin
Institute for the Study of Earth and Man
Geophysical Laboratory
Southern Methodist University
Dallas, TX 75275

Prof. Robert B. Herrmann
Department of Earth & Atmospheric Sciences
St. Louis University
St. Louis, MO 63156

Prof. Bryan Isacks
Cornell University
Department of Geological Sciences
SNEE Hall
Ithaca, NY 14850

Dr. Rong-Song Jih
Teledyne Geotech
314 Montgomery Street
Alexandria, VA 22314

Prof. Lane R. Johnson
Seismographic Station
University of California
Berkeley, CA 94720

Prof. Alan Kafka
Department of Geology & Geophysics
Boston College
Chestnut Hill, MA 02167

Dr. Richard LaCoss
MIT-Lincoln Laboratory
M-200B
P. O. Box 73
Lexington, MA 02173-0073 (3 copies)

Prof. Fred K. Lamb
University of Illinois at Urbana-Champaign
Department of Physics
1110 West Green Street
Urbana, IL 61801

Prof. Charles A. Langston
Geosciences Department
403 Deike Building
The Pennsylvania State University
University Park, PA 16802

Prof. Thorne Lay
Institute of Tectonics
Earth Science Board
University of California, Santa Cruz
Santa Cruz, CA 95064

Prof. Arthur Lerner-Lam
Lamont-Doherty Geological Observatory
of Columbia University
Palisades, NY 10964

Dr. Christopher Lynnes
Teledyne Geotech
314 Montgomery Street
Alexandria, VA 22314

Prof. Peter Malin
University of California at Santa Barbara
Institute for Crustal Studies
Santa Barbara, CA 93106

Dr. Randolph Martin, III
New England Research, Inc.
76 Olcott Drive
White River Junction, VT 05001

Dr. Gary McCartor
Mission Research Corporation
735 State Street
P.O. Drawer 719
Santa Barbara, CA 93102 (2 copies)

Prof. Thomas V. McEvilly
Seismographic Station
University of California
Berkeley, CA 94720

Dr. Keith L. McLaughlin
S-CUBED
A Division of Maxwell Laboratory
P.O. Box 1620
La Jolla, CA 92038-1620

Prof. William Menke
Lamont-Doherty Geological Observatory
of Columbia University
Palisades, NY 10964

Stephen Miller
SRI International
333 Ravenswood Avenue
Box AF 116
Menlo Park, CA 94025-3493

Prof. Bernard Minster
IGPP, A-025
Scripps Institute of Oceanography
University of California, San Diego
La Jolla, CA 92093

Prof. Brian J. Mitchell
Department of Earth & Atmospheric Sciences
St. Louis University
St. Louis, MO 63156

Prof. David G. Simpson
Lamont-Doherty Geological Observatory
of Columbia University
Palisades, NY 10964

- Mr. Jack Murphy
S-CUBED, A Division of Maxwell Laboratory
11800 Sunrise Valley Drive
Suite 1212
Reston, VA 22091 (2 copies)

Dr. Jeffrey Stevens
S-CUBED
A Division of Maxwell Laboratory
P.O. Box 1620
La Jolla, CA 92038-1620

Dr. Bao Nguyen
GL/LWH
Hanscom AFB, MA 01731-5000

Prof. Brian Stump
Institute for the Study of Earth & Man
Geophysical Laboratory
Southern Methodist University
Dallas, TX 75275

Prof. John A. Orcutt
IGPP, A-025
Scripps Institute of Oceanography
University of California, San Diego
La Jolla, CA 92093

Prof. Jeremiah Sullivan
University of Illinois at Urbana-Champaign
Department of Physics
1110 West Green Street
Urbana, IL 61801

Prof. Keith Priestley
University of Cambridge
Bullard Labs, Dept. of Earth Sciences
Madingley Rise, Madingley Rd.
Cambridge CB3 0EZ, ENGLAND

Prof. Clifford Thurber
University of Wisconsin-Madison
Department of Geology & Geophysics
1215 West Dayton Street
Madison, WI 53706

Prof. Paul G. Richards
L-210
Lawrence Livermore National Laboratory
Livermore, CA 94550

Prof. M. Nafi Toksoz
Earth Resources Lab
Massachusetts Institute of Technology
42 Carleton Street
Cambridge, MA 02142

Dr. Wilmer Rivers
Teledyne Geotech
314 Montgomery Street
Alexandria, VA 22314

Prof. John E. Vidale
University of California at Santa Cruz
Seismological Laboratory
Santa Cruz, CA 95064

Prof. Charles G. Sammis
Center for Earth Sciences
University of Southern California
University Park
Los Angeles, CA 90089-0741

Prof. Terry C. Wallace
Department of Geosciences
Building #77
University of Arizona
Tucson, AZ 85721

Prof. Christopher H. Scholz
Lamont-Doherty Geological Observatory
of Columbia University
Palisades, NY 10964

Dr. Raymond Willeman
GL/LWH
Hanscom AFB, MA 01731-5000

Thomas J. Sereno, Jr.
Science Application Int'l Corp.
10260 Campus Point Drive
San Diego, CA 92121

Dr. Lorraine Wolf
GL/LWH
Hanscom AFB, MA 01731-5000

OTHERS (United States)

Dr. Monem Abdel-Gawad
Rockwell International Science Center
1049 Camino Dos Rios
Thousand Oaks, CA 91360

Prof. Keiiti Aki
Center for Earth Sciences
University of Southern California
University Park
Los Angeles, CA 90089-0741

Prof. Shelton S. Alexander
Geosciences Department
403 Deike Building
The Pennsylvania State University
University Park, PA 16802

Dr. Kenneth Anderson
BBNSTC
Mail Stop 14/1B
Cambridge, MA 02238

Dr. Ralph Archuleta
Department of Geological Sciences
University of California at Santa Barbara
Santa Barbara, CA 93102

J. Barker
Department of Geological Sciences
State University of New York
at Binghamton
Vestal, NY 13901

Dr. T.J. Bennett
S-CUBED
A Division of Maxwell Laboratory
11800 Sunrise Valley Drive, Suite 1212
Reston, VA 22091

Mr. William J. Best
907 Westwood Drive
Vienna, VA 22180

Dr. N. Biswas
Geophysical Institute
University of Alaska
Fairbanks, AK 99701

Dr. G.A. Bollinger
Department of Geological Sciences
Virginia Polytechnical Institute
21044 Derring Hall
Blacksburg, VA 24061

Dr. Stephen Bratt
Center for Seismic Studies
1300 North 17th Street
Suite 1450
Arlington, VA 22209

Michael Browne
Teledyne Geotech
3401 Shiloh Road
Garland, TX 75041

Mr. Roy Burger
1221 Serry Road
Schenectady, NY 12309

Dr. Robert Burrige
Schlumberger-Doll Research Center
Old Quarry Road
Ridgefield, CT 06877

Dr. Jerry Carter
Rondout Associates
P.O. Box 224
Stone Ridge, NY 12484

Dr. W. Winston Chan
Teledyne Geotech
314 Montgomery Street
Alexandria, VA 22314-1581

Dr. Theodore Cherry
Science Horizons, Inc.
710 Encinitas Blvd., Suite 200
Encinitas, CA 92024 (2 copies)

Prof. Jon F. Claerbout
Department of Geophysics
Stanford University
Stanford, CA 94305

Prof. Robert W. Clayton
Seismological Laboratory
Division of Geological & Planetary Sciences
California Institute of Technology
Pasadena, CA 91125

Prof. F. A. Dahlen
Geological and Geophysical Sciences
Princeton University
Princeton, NJ 08544-0636

Prof. Adam Dziewonski
Hoffman Laboratory
Harvard University
20 Oxford St
Cambridge, MA 02138

Prof. John Ebel
Department of Geology & Geophysics
Boston College
Chestnut Hill, MA 02167

Eric Fielding
SNEE Hall
INSTOC
Cornell University
Ithaca, NY 14853

Prof. Donald Forsyth
Department of Geological Sciences
Brown University
Providence, RI 02912

Dr. Cliff Frolich
Institute of Geophysics
8701 North Mopac
Austin, TX 78759

Dr. Anthony Gangi
Texas A&M University
Department of Geophysics
College Station, TX 77843

Dr. Freeman Gilbert
Inst. of Geophysics & Planetary Physics
University of California, San Diego
P.O. Box 109
La Jolla, CA 92037

Mr. Edward Giller
Pacific Sierra Research Corp.
1401 Wilson Boulevard
Arlington, VA 22209

Dr. Jeffrey W. Given
SAIC
10260 Campus Point Drive
San Diego, CA 92121

Prof. Roy Greenfield
Geosciences Department
403 Deike Building
The Pennsylvania State University
University Park, PA 16802

Dan N. Hagedorn
Battelle
Pacific Northwest Laboratories
Battelle Boulevard
Richland, WA 99352

Kevin Hutchenson
Department of Earth Sciences
St. Louis University
3507 Laclede
St. Louis, MO 63103

Prof. Thomas H. Jordan
Department of Earth, Atmospheric
and Planetary Sciences
Massachusetts Institute of Technology
Cambridge, MA 02139

Robert C. Kemerait
ENSCO, Inc.
445 Pineda Court
Melbourne, FL 32940

William Kikendall
Teledyne Geotech
3401 Shiloh Road
Garland, TX 75041

Prof. Leon Knopoff
University of California
Institute of Geophysics & Planetary Physics
Los Angeles, CA 90024

Prof. L. Timothy Long
School of Geophysical Sciences
Georgia Institute of Technology
Atlanta, GA 30332

Prof. Art McGarr
Mail Stop 977
Geological Survey
345 Middlefield Rd.
Menlo Park, CA 94025

Dr. George Mellman
Sierra Geophysics
11255 Kirkland Way
Kirkland, WA 98033

Prof. John Nabelek
College of Oceanography
Oregon State University
Corvallis, OR 97331

Prof. Geza Nagy
University of California, San Diego
Department of Ames, M.S. B-010
La Jolla, CA 92093

Prof. Amos Nur
Department of Geophysics
Stanford University
Stanford, CA 94305

Prof. Jack Oliver
Department of Geology
Cornell University
Ithaca, NY 14850

Prof. Robert Phinney
Geological & Geophysical Sciences
Princeton University
Princeton, NJ 08544-0636

Dr. Paul Pomeroy
Rondout Associates
P.O. Box 224
Stone Ridge, NY 12484

Dr. Jay Pulli
RADIX System, Inc.
2 Taft Court, Suite 203
Rockville, MD 20850

Dr. Norton Rimer
S-CUBED
A Division of Maxwell Laboratory
P.O. Box 1620
La Jolla, CA 92038-1620

Prof. Larry J. Ruff
Department of Geological Sciences
1006 C.C. Little Building
University of Michigan
Ann Arbor, MI 48109-1063

Dr. Richard Sailor
TASC Inc.
55 Walkers Brook Drive
Reading, MA 01867

John Sherwin
Teledyne Geotech
3401 Shiloh Road
Garland, TX 75041

Prof. Robert Smith
Department of Geophysics
University of Utah
1400 East 2nd South
Salt Lake City, UT 84112

Dr. Stewart W. Smith
Geophysics AK-50
University of Washington
Seattle, WA 98195

Dr. George Sutton
Rondout Associates
P.O. Box 224
Stone Ridge, NY 12484

Prof. L. Sykes
Lamont-Doherty Geological Observatory
of Columbia University
Palisades, NY 10964

Prof. Pradeep Talwani
Department of Geological Sciences
University of South Carolina
Columbia, SC 29208

Prof. Ta-liang Teng
Center for Earth Sciences
University of Southern California
University Park
Los Angeles, CA 90089-0741

Dr. R.B. Tittmann
Rockwell International Science Center
1049 Camino Dos Rios
P.O. Box 1085
Thousand Oaks, CA 91360

Dr. Gregory van der Vink
IRIS, Inc.
1616 North Fort Myer Drive
Suite 1440
Arlington, VA 22209

Professor Daniel Walker
University of Hawaii
Institute of Geophysics
Honolulu, HI 96822

William R. Walter
Seismological Laboratory
University of Nevada
Reno, NV 89557

- Dr. Gregory Wojcik
Weidlinger Associates
4410 El Camino Real
- Suite 110
Los Altos, CA 94022

Prof. John H. Woodhouse
Hoffman Laboratory
Harvard University
20 Oxford St.
Cambridge, MA 02138

Prof. Francis T. Wu
Department of Geological Sciences
State University of New York
at Binghamton
Vestal, NY 13901

Dr. Gregory B. Young
ENSCO, Inc.
5400 Port Royal Road
Springfield, VA 22151-2388

GOVERNMENT

Dr. Ralph Alewine III
DARPA/NMRO
1400 Wilson Boulevard
Arlington, VA 22209-2308

Mr. James C. Battis
GL/LWH
Hanscom AFB, MA 01731-5000

Dr. Robert Blandford
DARPA/NMRO
1400 Wilson Boulevard
Arlington, VA 22209-2308

Eric Chael
Division 9241
Sandia Laboratory
Albuquerque, NM 87185

Dr. John J. Cipar
GL/LWH
Hanscom AFB, MA 01731-5000

Mr. Jeff Duncan
Office of Congressman Markey
2133 Rayburn House Bldg.
Washington, DC 20515

Dr. Jack Evernden
USGS - Earthquake Studies
345 Middlefield Road
Menlo Park, CA 94025

Art Frankel
USGS
922 National Center
Reston, VA 22092

Dr. T. Hanks
USGS
Nat'l Earthquake Research Center
345 Middlefield Road
Menlo Park, CA 94025

Dr. James Hannon
Lawrence Livermore Nat'l Laboratory
P.O. Box 808
Livermore, CA 94550

Paul Johnson
ESS-4, Mail Stop J979
Los Alamos National Laboratory
Los Alamos, NM 87545

Janet Johnston
GL/LWH
Hanscom AFB, MA 01731-5000

Dr. Katharine Kadinsky-Cade
GL/LWH
Hanscom AFB, MA 01731-5000

Ms. Ann Kerr
IGPP, A-025
Scripps Institute of Oceanography
University of California, San Diego
La Jolla, CA 92093

Dr. Max Koontz
US Dept of Energy/DP 5
Forrestal Building
1000 Independence Avenue
Washington, DC 20585

Dr. W.H.K. Lee
Office of Earthquakes, Volcanoes,
& Engineering
345 Middlefield Road
Menlo Park, CA 94025

Dr. William Leith
U.S. Geological Survey
Mail Stop 928
Reston, VA 22092

Dr. Richard Lewis
Director, Earthquake Engineering & Geophysics
U.S. Army Corps of Engineers
Box 631
Vicksburg, MS 39180

James F. Lewkowicz
GL/LWH
Hanscom AFB, MA 01731-5000

Mr. Alfred Lieberman
ACDA/VI-OA State Department Bldg
Room 5726
320 - 21st Street, NW
Washington, DC 20451

Stephen Mangino
GL/LWH
Hanscom AFB, MA 01731-5000

Dr. Frank F. Pilotte
HQ AFTAC/TT
Patrick AFB, FL 32925-6001

Dr. Robert Masse
Box 25046, Mail Stop 967
Denver Federal Center
Denver, CO 80225

Katie Poley
CIA-OSWR/NED
Washington, DC 20505

Art McGarr
U.S. Geological Survey, MS-977
345 Middlefield Road
Menlo Park, CA 94025

Mr. Jack Rachlin
U.S. Geological Survey
Geology, Rm 3 C136
Mail Stop 928 National Center
Reston, VA 22092

Richard Morrow
ACDA/VI, Room 5741
320 21st Street N.W.
Washington, DC 20451

Dr. Robert Reinke
WL/NTESG
Kirtland AFB, NM 87117-6008

Dr. Keith K. Nakanishi
Lawrence Livermore National Laboratory
P.O. Box 808, L-205
Livermore, CA 94550

Dr. Byron Ristvet
HQ DNA, Nevada Operations Office
Attn: NVCG
P.O. Box 98539
Las Vegas, NV 89193

Dr. Carl Newton
Los Alamos National Laboratory
P.O. Box 1663
Mail Stop C335, Group ESS-3
Los Alamos, NM 87545

Dr. George Rothe
HQ AFTAC/TGR
Patrick AFB, FL 32925-6001

Dr. Kenneth H. Olsen
Los Alamos Scientific Laboratory
P.O. Box 1663
Mail Stop C335, Group ESS-3
Los Alamos, NM 87545

Dr. Alan S. Ryall, Jr.
DARPA/NMRO
1400 Wilson Boulevard
Arlington, VA 22209-2308

Howard J. Patton
Lawrence Livermore National Laboratory
P.O. Box 808, L-205
Livermore, CA 94550

Dr. Michael Shore
Defense Nuclear Agency/SPSS
6801 Telegraph Road
Alexandria, VA 22310

Mr. Chris Paine
Office of Senator Kennedy
SR 315
United States Senate
Washington, DC 20510

Dr. Aibert Smith
Los Alamos National Laboratory
L-205
P. O. Box 808
Livermore, CA 94550

Colonel Jerry J. Perrizo
AFOSR/NP, Building 410
Bolling AFB
Washington, DC 20332-6448

Donald L. Springer
Lawrence Livermore National Laboratory
L-205
P. O. Box 808
Livermore, CA 94550

Mr. Charles L. Taylor
GL/LWG
Hanscom AFB, MA 01731-5000

DARPA/RMO/Security Office
1400 Wilson Boulevard
Arlington, VA 22209

Mr. Steven R. Taylor
Lawrence Livermore National Laboratory
L-205
P. O. Box 808
Livermore, CA 94550

Geophysics Laboratory
Attn: XO
Hanscom AFB, MA 01731-5000

Dr. Eileen Vergino
Lawrence Livermore National Laboratory
L-205
P. O. Box 808
Livermore, CA 94550

Geophysics Laboratory
Attn: LW
Hanscom AFB, MA 01731-5000

Dr. Thomas Weaver
Los Alamos National Laboratory
P.O. Box 1663, Mail Stop C335
Los Alamos, NM 87545

DARPA/PM
1400 Wilson Boulevard
Arlington, VA 22209

J.J. Zucca
Lawrence Livermore National Laboratory
P. O. Box 808
Livermore, CA 94550

Defense Technical Information Center
Cameron Station
Alexandria, VA 22314 (5 copies)

GL/SULL
Research Library
Hanscom AFB, MA 01731-5000 (2 copies)

Defense Intelligence Agency
Directorate for Scientific
& Technical Intelligence Attn: DT1B
Washington, DC 20340-6158

Secretary of the Air Force
(SAFRD)
Washington, DC 20330

AFTAC/CA
(STINFO)
Patrick AFB, FL 32925-6001

Office of the Secretary Defense
DDR & E
Washington, DC 20330

TACTEC
Battelle Memorial Institute
505 King Avenue
Columbus, OH 43201 (Final Report Only)

HQ DNA
Attn: Technical Library
Washington, DC 20305

DARPA/RMO/RETRIEVAL
1400 Wilson Boulevard
Arlington, VA 22209

CONTRACTORS (Foreign)

Dr. Ramon Cabre, S.J.
Observatorio San Calixto
Casilla 5939
La Paz, Bolivia

• Prof. Hans-Peter Harjes
Institute for Geophysik
Ruhr University/Bochum
• P.O. Box 102148
4630 Bochum 1, FRG

Prof. Eystein Husebye
NTNF/NORSAR
P.O. Box 51
N-2007 Kjeller, NORWAY

Prof. Brian L.N. Kennett
Research School of Earth Sciences
Institute of Advanced Studies
G.P.O. Box 4
Canberra 2601, AUSTRALIA

Dr. Bernard Massinon
Societe Radiomana
27 rue Claude Bernard
75005 Paris, FRANCE (2 Copies)

Dr. Pierre Mecheler
Societe Radiomana
27 rue Claude Bernard
75005 Paris, FRANCE

Dr. Svein Mykkeltveit
NTNF/NORSAR
P.O. Box 51
N-2007 Kjeller, NORWAY

FOREIGN (Others)

Dr. Peter Basham
Earth Physics Branch
Geological Survey of Canada
1 Observatory Crescent
Ottawa, Ontario, CANADA K1A 0Y3

Dr. Eduard Berg
Institute of Geophysics
University of Hawaii
Honolulu, HI 96822

Dr. Michel Bouchon
I.R.I.G.M.-B.P. 68
38402 St. Martin D'Herès
Cedex, FRANCE

Dr. Hilmar Bungum
NTNF/NORSAR
P.O. Box 51
N-2007 Kjeller, NORWAY

Dr. Michel Campillo
Observatoire de Grenoble
I.R.I.G.M.-B.P. 53
38041 Grenoble, FRANCE

Dr. Kin Yip Chun
Geophysics Division
Physics Department
University of Toronto
Ontario, CANADA M5S 1A7

Dr. Alan Douglas
Ministry of Defense
Blacknest, Brimpton
Reading RG7-4RS, UNITED KINGDOM

Dr. Roger Hansen
NTNF/NORSAR
P.O. Box 51
N-2007 Kjeller, NORWAY

Dr. Manfred Henger
Federal Institute for Geosciences & Nat'l Res.
Postfach 510153
D-3000 Hanover 51, FRG

Ms. Eva Johannisson
Senior Research Officer
National Defense Research Inst.
P.O. Box 27322
S-102 54 Stockholm, SWEDEN

Dr. Fekadu Kebede
Seismological Section
Box 12019
S-750 Uppsala, SWEDEN

Dr. Tormod Kvaerna
NTNF/NORSAR
P.O. Box 51
N-2007 Kjeller, NORWAY

Dr. Peter Marshal
Procurement Executive
Ministry of Defense
Blacknest, Brimpton
Reading FG7-4RS, UNITED KINGDOM

Prof. Ari Ben-Menahem
Department of Applied Mathematics
Weizman Institute of Science
Rehovot, ISRAEL 951729

Dr. Robert North
Geophysics Division
Geological Survey of Canada
1 Observatory Crescent
Ottawa, Ontario, CANADA K1A 0Y3

Dr. Frode Ringdal
NTNF/NORSAR
P.O. Box 51
N-2007 Kjeller, NORWAY

Dr. Jorg Schlittenhardt
Federal Institute for Geosciences & Nat'l Res.
Postfach 510153
D-3000 Hannover 51, FEDERAL REPUBLIC OF
GERMANY